

Accepted Manuscript

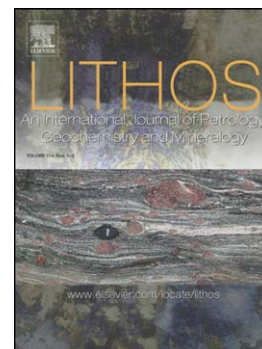
The Petrogenesis of the Early Permian Variscan granites of the Cornubian Batholith – lower plate post-collisional peraluminous magmatism in the Rhenohercynian Zone of SW England

B. Simons, Robin K. Shail, Jens C.Ø. Andersen

PII: S0024-4937(16)30095-0
DOI: doi: [10.1016/j.lithos.2016.05.010](https://doi.org/10.1016/j.lithos.2016.05.010)
Reference: LITHOS 3928

To appear in: *LITHOS*

Received date: 29 February 2016
Accepted date: 23 May 2016



Please cite this article as: Simons, B., Shail, Robin K., Andersen, Jens C.Ø., The Petrogenesis of the Early Permian Variscan granites of the Cornubian Batholith – lower plate post-collisional peraluminous magmatism in the Rhenohercynian Zone of SW England, *LITHOS* (2016), doi: [10.1016/j.lithos.2016.05.010](https://doi.org/10.1016/j.lithos.2016.05.010)

This is a PDF file of an unedited manuscript that has been accepted for publication. As a service to our customers we are providing this early version of the manuscript. The manuscript will undergo copyediting, typesetting, and review of the resulting proof before it is published in its final form. Please note that during the production process errors may be discovered which could affect the content, and all legal disclaimers that apply to the journal pertain.

The Petrogenesis of the Early Permian Variscan granites of the Cornubian Batholith – lower plate post-collisional peraluminous magmatism in the Rhenohercynian Zone of SW England.

B. Simons^{1*}, Robin K. Shail¹, Jens C.Ø. Andersen¹

¹Camborne School of Mines, University of Exeter, Penryn Campus, Penryn, Cornwall,
United Kingdom, TR10 9FE

*Corresponding author: Bethany Simons (B.Simons@exeter.ac.uk)

Keywords: Granite; geochemistry; petrogenesis; peraluminous; Variscan; Rhenohercynian
Zone

ABSTRACT

The Early Permian Cornubian Batholith was generated during an extensional regime following Variscan convergence within the Rheohercynian Zone of SW England. Its component granites can be classified, using mineralogical, textural and geochemical criteria, into five main types, all of which are peraluminous ($A/CNK > 1.1$): G1 (two-mica), G2 (muscovite), G3 (biotite), G4 (tourmaline) and G5 (topaz). G1 granites formed through up to 20% muscovite and minor biotite dehydration melting of a metagreywacke source at moderate temperatures and pressures (731-806°C, >5 kbar). Younger G3 granites formed through higher temperature, lower pressure (768-847°C, <4 kbar) biotite-dominated melting of a similar source. Partial melting was strongly influenced by the progressive lower-mid crustal emplacement of mafic igneous rocks during post-Variscan extension and a minor (<5-10%) mantle-derived component in the granites is possible. Two distinct fractionation series, G1-G2 and G3-G4, are defined using whole rock geochemical and mineral chemical data. Variations in the major elements, Ba, Sr and Rb indicate that G1 and G3 granites underwent 15-30% fractionation of an assemblage dominated by plagioclase, alkali feldspar and biotite to form, more evolved G2 and G4 granites respectively. Decreasing whole rock abundances of Zr, Th and REE support fractionation of zircon, monazite, apatite and allanite. Subsolidus alteration in G2 and G4 granites is indicated by non-primary muscovite and tourmaline and modification of major and trace element trends for G3-G4 granites, particularly for P_2O_5 and Rb. Topaz (G5) granites show low Zr, REE and extreme enrichment in Rb (up to 1530 ppm) and Nb (79 ppm) that cannot be related in a straightforward manner to continued differentiation of the G1-G2 or G3-G4 series. Instead, they are considered to represent partial melting, mediated by granulite facies fluids, of a biotite-rich restite following extraction of

G1 and/or G3 magmas; they do not exhibit the typical geochemical characteristics of intraplate A-type granites.

ACCEPTED MANUSCRIPT

1. INTRODUCTION

Peraluminous granites, derived predominantly from partial melting of muscovite- and/or biotite-bearing metasedimentary source rocks, are commonly generated within tectonically thickened crust during, or immediately after, continental collision (e.g. Bonin et al., 1998; Sylvester, 1998). These granites are usually emplaced in the upper crust and are associated with high concentrations of fluxing elements (Li, F, B, P) and economic metals such as Sn, Nb, Ta and W that may result in magmatic and/or magmatic-hydrothermal mineralisation (e.g. Černý et al., 2005).

Various models have been proposed for the geochemical evolution of peraluminous granites including source variation (e.g. Nabelek and Bartlett, 1999), varying degrees of partial melting (e.g. Harris et al., 1995), incorporation of restite material or a peritectic phase (e.g. Chappell et al., 1987), mixing with mantle-derived melts (e.g. Patiño-Douce, 1999), wall-rock assimilation (e.g. DePaolo, 1981), fluid overprint (e.g. Haapala, 1997) and fractional crystallisation (e.g. Teixeira et al., 2012). Ultimately, granite compositional characteristics may reflect several processes.

The Variscan granites of the Cornubian Batholith of SW England are commonly used as a global reference for granite genesis and associated magmatic-hydrothermal mineralisation (Willis-Richards and Jackson, 1989; Chappell and Hine, 2006). The granites were generated and emplaced during a 20 Ma period of Early Permian post-collisional extension but, in contrast to most Variscan granites, north of the Rheic suture within the lower plate Rheohercynian Zone (RHZ) (Shail and Leveridge, 2009). Such distinctiveness is recognised in the recent definition of a 'Cornwall-type' setting for granite magmatism and tin mineralisation associated with early post-orogenic extension (Romer and Kroner, 2015, 2016).

The purpose of this study is to evaluate the petrogenetic controls on the development of a diverse suite of peraluminous granites in a post-collisional tectonic setting, assessing the mechanisms controlling geochemical evolution. In doing so, we present the first integrated petrogenetic analysis for 20 years of all the component granite types within the Cornubian Batholith. The spatial and temporal distribution of granite types and their relations to source characteristics, partial melting conditions, fractional crystallisation and the role of mantle-derived melts are all evaluated. We combine mineralogical and mineral chemical data with major and trace element geochemical data and geochemical modelling, based on melting experiments performed on a range of source rock types (Holtz and Johannes, 1991; Montel and Vielzeuf, 1997; Patiño-Douce, 1999), to present: (1) a revised classification of component granite types, and (2) a new petrogenetic model for the Cornubian Batholith.

2. GEOLOGICAL SETTING

The Early Permian Cornubian Batholith is hosted by Devonian and Carboniferous successions of the SW England Variscan massif that are correlated with the RHZ of the Variscan orogen (e.g. Shail and Leveridge, 2009; Nance et al., 2010). These successions were deposited during the development of a southwards-facing passive margin to either a short-lived marginal or successor basin to the Rheic Ocean. Southwest England occupied a lower plate position during late Devonian convergence; continental collision initiated in the earliest Carboniferous and Variscan shortening migrated northwards through the passive margin (Franke, 2000; Shail and Leveridge, 2009). The youngest deformed successions are late Carboniferous (Moscovian) in age (Edwards et al., 1997). Regional metamorphism of all Devonian-Carboniferous successions seldom exceeds very low grade (epizone-anchizone) (Warr et al., 1991).

Variscan convergence ceased during the late Carboniferous and was replaced across NW Europe by a dextral transtensional regime (Ziegler and Dèzes, 2006). In SW England, this was manifested by the latest Carboniferous to Early Permian reactivation of Variscan thrusts, and development of new fault systems, during NNW-SSE lithospheric extension (Shail and Alexander, 1997). Thinning and exhumation of lower plate SW England, during extensional reactivation of the Rhenohercynian suture, was accompanied by Early Permian post-collisional magmatism, magmatic-hydrothermal mineralisation and the development of 'red-bed' sedimentary basins (Shail and Wilkinson, 1994).

The Cornubian Batholith is exposed in a series of six major plutons and several minor stocks from the Isles of Scilly in the west to Dartmoor in the east (Figure 1). Gravity anomaly data indicate that the batholith is continuous at depth (Bott et al., 1958), 250 km long, 20-40 km wide and 10 km thick around Dartmoor, but possibly 5-6 km farther west (Taylor, 2007), implying the generation and emplacement of *c.* 40,000 km³ of magma.

The batholith is composite and displays considerable mineralogical and textural variation (e.g. Dangerfield and Hawkes, 1981; Stimac et al., 1995; Manning et al., 1996). Field observations indicate that individual magma batches were accumulated as sheet-like intrusions (e.g. Müller et al., 2006a). All granites post-date host rock structures developed during Variscan convergence and largely post-date those attributable to post-Variscan extensional reactivation of thrusts (Shail and Alexander, 1997). The older plutons >289 Ma (Bodmin, Carnmenellis, Isles of Scilly) exhibit localised magmatic and solid state fabrics (e.g. Bouchez et al., 2006), whereas younger plutons (Dartmoor, St Austell, Land's End) exhibit only magmatic state fabrics (e.g. Kratinová et al., 2010); both fabrics indicate some degree of coupling with extensional host rock deformation.

Associated with the batholith are substantial rhyolite / microgranite intrusive sheets (known locally as 'elvans') and remnants of formerly more extensive felsic lavas and

pyroclastic rocks (Awad et al., 1996). Contemporaneous mafic lavas occur at or near the base of post-Variscan Permian 'red-beds' and as intrusive sheets within Variscan-deformed Devonian-Carboniferous successions (Dupuis et al., 2015). U-Pb monazite and xenotime ages indicate almost 20 Ma of magmatic activity from 293.9 ± 0.6 Ma (Carmenellis Granite) to 274.4 ± 0.4 Ma (Land's End Granite) (Chesley et al., 1993; Clark et al., 1994).

3. Sampling and analytical methodology

Samples represent all of the different granite types within the region. The majority were collected from working and disused quarries, with the remaining collected from outcrop or drill core. Sampling close to mineralised lodes and extensively kaolinised outcrops were generally avoided. Additional Land's End Granite specimens from the study of Müller et al. (2006a) were obtained from the Natural History Museum, London.

Mineral chemistry was determined with the JEOL JXA-8200 superprobe at Camborne School of Mines, using an accelerating voltage of 15 kV and a beam current of 1.5×10^{-8} A. The instrument was calibrated using natural silicate minerals supplied by Astimex Ltd. AST-biotite was utilised as a secondary standard. Detection limits were determined per analysis, generally $<0.02\%$ for most elements, and the precision was $<5\%$.

Whole rock major and trace element data (Ba, Cu, Ga, Pb, Rb, Sr, Th, U, V, Y, Zn and Zr) were determined by XRF analysis at Activation Laboratories, Canada. Samples were prepared as fused beads for major elements and pressed pellets for trace elements. Further trace elements (Nb and REE) were determined using the Agilent 7700 ICP-MS at Camborne School of Mines. Samples were digested in PTFE tubes using HF, HNO₃, HClO₃ and HCl following the procedure of Yu et al. (2001). Detection limits were taken as 10 times the standard deviation of 10 blanks (typically <0.5 ppm) and precision is $<10\%$. International

standard reference material and internal standards (GSP-2, BIR-1a) show excellent agreement with certified and preferred values.

4. Petrology

4.1. Textures and mode of occurrence

Previous studies (Exley and Stone, 1964; Dangerfield and Hawkes, 1981) provide a field-based classification scheme that covers the range of granite types across the region. These schemes classify the granites by the occurrence of biotite or tourmaline as the dominant ferromagnesian mineral, size and abundance of alkali feldspar phenocrysts and a fine- (<1 mm), medium- (1-2 mm) or a coarse-grained (>2 mm) groundmass. The tourmaline granites can be further subdivided into three textural subtypes: globular quartz, equigranular and lithium-mica variants; each named for their distinctive textural characteristics (Manning et al., 1996). These classifications are adapted for this study, providing five granite types that have unique textural, mineralogical and geochemical characteristics (Table 1, Figure 1).

Two mica (G1) granite (Figure 2a) is the dominant lithology of the Bodmin, Carnmenellis and Isles of Scilly plutons. G1 granites are fine- to coarse-grained with microperthitic feldspar phenocrysts up to 25 mm and approximately equal abundances of biotite and muscovite mica. Accessory minerals include andalusite, zircon, apatite, monazite, rutile and widespread late-stage tourmaline. Muscovite (G2) granite is texturally similar to G1 granite with microperthitic alkali feldspar phenocrysts, plagioclase and late-stage tourmaline but muscovite is dominant over biotite (Figure 2b). Muscovite occurs as both a primary magmatic and a replacive subsolidus mineral in both G1 and G2. G2 granite is

confined to small stocks (St. Michael's Mount, Cligga, Kit Hill, Hingston Down and Hemerdon). G1 and G2 granites are typically >282 Ma (Clark et al., 1994).

Biotite (G3) granite is the dominant lithology in the younger (<282 Ma) Dartmoor, St. Austell and Land's End plutons. G3 granites are fine- to coarse-grained, with microperthitic alkali feldspar phenocrysts >25 mm, approximately 10% modal biotite, plagioclase and accessory tourmaline, cordierite, zircon, monazite, apatite and rutile (Figure 2c). Tourmaline (G4) granites have distinct textural variants, described in detail by Manning et al. (1996); globular quartz (Figure 2d), equigranular and a coarse-grained Li-mica porphyritic facies that is texturally similar to coarse-grained porphyritic two mica (G1a) granites. G4 granites are usually characterised by tourmaline as the dominant ferromagnesian mineral, with Li-rich biotite group micas and accessory topaz, apatite, columbite and Nb-rich rutile / ilmenite.

Topaz (G5) granite is equigranular with very rare alkali feldspar phenocrysts, tourmaline and up to 3% modal topaz (Figure 2e). Plagioclase is almost pure albite and biotite group micas are Li-rich, trending towards lepidolite compositions. Accessory minerals are low in abundance, but diverse, comprising amblygonite, Nb-rich rutile, Mn-rich apatite, columbite-tantalite, cassiterite, zircon, fluorite and very rare wolframite. Topaz-rich aplites and pegmatites are associated with the Tregonning and St. Austell G5 granites (Stone, 1975, 1992; Manning et al., 1996).

Contacts between varying granite types are variable and reflect the composite nature of the batholith. Boundaries between tourmaline (G4) granites within St. Austell Granite are gradational, as are contacts between porphyritic and poorly porphyritic biotite (G3) granites at Porth Ledden, Land's End Granite. Fine-grained G1 and G3 granites commonly form sharp contacts with adjacent porphyritic granites but also occur as enclaves within coarser-grained varieties (Figure 3a-b). These fine-grained granite enclaves are typically globular showing undulose boundaries with the enclosing granite. Accumulation of K-feldspar

phenocrysts is also widespread, particularly in G3 granites, occurring in turbulent swirls or defining magmatic state fabrics (Figure 3c).

Inclusions within the granites include country rock xenolith, non-igneous enclaves (NIE) and microgranular mafic enclaves (MME) (e.g. Stimac et al. 1995). Country rock xenoliths show sharp contacts with the granites and retain metasedimentary structures, such as a cleavage (Figure 3d). Mafic enclaves display textures typical of magma mingling, possessing lobate contacts with the enclosing granite (Figure 3e). These MME often contain alkali feldspar phenocrysts protruding from the enclosing granite.

4.2 Mineral characteristics and chemistry

Major mineral chemistry has been used to document granite evolution in several granite terrains. Variations in the mineral chemistry of plagioclase and mica within the Variscan granites of Germany and Portugal indicate melt composition at the time of crystallisation and reflect the evolution of the host granite (e.g. Förster et al., 1999; Neiva et al., 2011). Complete mineral chemistry data are provided in Supplementary Table 1.

4.2.1. Quartz

Quartz is anhedral with an allotriomorphic texture in G1, G2, G3 and G5. It has no dominant mineral association, forming interstitial grains between plagioclase and alkali feldspar and composite grains. Undulose extinction is exhibited in >60% of samples across all granites types, with recrystallized grains in older plutons. Inclusions of mica, feldspar and rutile are disseminated throughout individual grains, rarely in oscillatory zoned patterns in hydrothermally altered samples of G2 and G4. Granophyric textures are widespread

throughout G3 granites. The G1a Isles of Scilly Granite displays myrmekitic textures, probably a consequence of ductile deformation, and “ribbon” quartz locally occurs within G1 granite samples from the Bodmin Moor and Isles of Scilly plutons. Globular quartz phenocrysts within G4 granites are rich in fluid inclusions and fractures, with white mica infill in between the individual grains.

4.2.3. *Micas*

Biotite group micas are anhedral to subhedral and, in G1 and G3 granites, dark brown, pleochroic, and contain numerous inclusions of zircon and monazite that result in host grain metamictisation (Figure 4a). Within G2, G4 and G5 granites, biotite group minerals are pale pink with inclusions (Figure 4b). Individual grains and “patches” of biotite are common. Chlorite alteration of biotite is widespread and of variable extent, but is particularly common along cleavage. There is a wide variation in mica composition across the Cornubian Batholith that reflects the geochemical evolution of the different granite types (e.g. Stone et al., 1988; Henderson and Martin, 1989). The mica formulas have been calculated to 22 oxygen atoms and the Li_2O content calculated according to Tischendorf et al. (1997). All biotites are trioctahedral, consistent with the previous studies of Stone et al. (1988), as the octahedral Y-site always contains more than 5 atoms per 11 oxygen atoms and the interlayer cation site atoms have a total of approximately 2. Mica names are in accordance with the IUGS classification of Rieder et al. (1998).

Within G1 and G3 biotite granites, magnesian siderophyllite or siderophyllite are the common biotite compositions. These micas are rich in Fe (17-22 wt.% FeO), Ti (2-3 wt.% TiO_2) and Mg (3-4 wt.% MgO) (Figure 5a). Smaller stocks of G2 granite, such as Cligga, Kit Hill, Carn Marth and Castle-an-Dinas (Land’s End), have pale brown lithian siderophyllite as

the primary trioctahedral mica. Lithian siderophyllite is dominant within the G4 lithium mica subdivision. Other G4 tourmaline granites (equigranular, globular quartz) and G5 granites contain pale pink zinnwaldite and lepidolite (Figure 4b). Mica compositions reflect a differentiation continuum, revealed by increasing Li content with decreasing Fe, Mg and Ti (Figure 5a). The geochemical continuum demonstrated by biotite chemistry (magnesium siderophyllite to zinnwaldite) from the least (G1, G3) to the most (G2, G4) evolved granites, is supported by major and trace element whole-rock geochemistry.

Muscovite comprises up to 5% of G1 biotite granites and is approximately equal in modal abundance to biotite. Muscovite is dominant in the volumetrically smaller G2 muscovite granites reaching up to 10% modal abundance (Figure 4c). In G3, G4 and G5 granites, muscovite is an accessory mineral. In G1 and G2 granites, muscovite occurs as: (1) subhedral disseminated magmatic grains containing inclusions of radioactive and opaque minerals that have caused metamictisation, and (2) anhedral to subhedral subsolidus grains mantling biotite, along feldspar twin planes and in large (>4 mm) aggregate “patches”.

When muscovite is present in samples with either siderophyllite or magnesium siderophyllite, the major element composition trends towards pure muscovite. In samples with lithian siderophyllite, where muscovite is often the dominant mica, muscovite compositions show higher degrees of trioctahedral substitution and trend towards ferroan muscovite or lithium ferroan muscovite; the latter is the common composition of muscovite mantling biotite (Figure 5a).

4.2.1. Plagioclase

Plagioclase is subhedral to euhedral (tabular), with abundances of up to 20% in G1, G2 and G3 biotite granites and 35% in G4 and G5 granites. Polysynthetic twinning (Albite

law), concentric zoning on basal sections and white mica alteration, particularly towards the centre of grains, is widespread across all granite types. There is a marked variation in plagioclase composition between the different granite types and plagioclase cores are more calcic than crystal rims (Table 2; Figure 5b). The more evolved G2, G4 and G5 granites have plagioclase compositions of almost pure albite ($Ab > 96$).

4.2.2. Alkali feldspar

Alkali feldspar, both phenocrysts and groundmass, is orthoclase and comprises ~30% modal abundance in G1, G2 and G3 granites and 25% in G4 and G5 granites. Microperthitic phenocrysts attain lengths of 150 μ m and are euhedral tabular displaying Carlsbad twinning. Concentric zoned inclusions of plagioclase, quartz, micas and opaques are common in phenocrysts (Figure 4d). For major element data there is no variation between the core and rim of phenocrysts (Table 2). Microperthite within phenocrysts trends towards albite compositions and shows limited variation across different granite types ($Or_{1-3}Ab_{93-98}An_{0-5}$).

4.2.5. Tourmaline

The tourmaline abundance in G1, G2, G3 and G5 granites ranges from <1% to 3% but it is the dominant ferromagnesian mineral in G4 granites reaching 5%. In all granite types, tourmaline shows limited concentric zoning from pale yellow cores to dark yellow and, occasionally, blue rims (Figure 4e). Inclusions of zircon, apatite and Th-rich monazite result in metamictisation, visible with a blue halo. Tourmaline also occurs as disseminated individual grains and in quartz-tourmaline orbicules, the latter being common in G3 granites (Drivenes et al., 2015). The majority of the tourmaline is schorl with the rims of tourmaline

from aplites and topaz granites occasionally reaching elbaite compositions, consistent with the study by London and Manning (1995). The parameter $Mg/(Mg+Fe)$ decreases with granite evolution, and G2, G4 and G5 granites show the lowest $Mg/(Mg+Fe)$.

4.2.6. Accessory minerals

Cordierite is a widespread accessory mineral in G3 biotite granites and occurs as pinitite-altered subhedral grains, rarely showing “sixling” twinning (Figure 4f). Cornubian cordierite contains less Mg than cordierite reported from other S-type granites (Erdmann et al., 2009). A $Mg/(Mg+Fe+Mn)$ ratio of 0.53-0.57 and total channel cations (Na, Ca and K) of 0.21-0.25 place the cordierite well within the primary magmatic cordierite field of Pereira and Bea (1994) and are consistent with textural observations.

G1, G2 and G5 granites have white-mica altered andalusite which is almost always associated with tourmaline, rarely with biotite (Figure 4e). Grains are subhedral, with euhedral pink pleochroic cores, reaching 3 mm in length. Apatite and zircon are commonly included within micas; both are subhedral to euhedral. The abundance of zircon is higher in G1 and G3 granites with apatite more abundant in G2, G4 and G5 granites than in the former. Fe- or Ti-rich accessory minerals are dominated by ilmenite and rutile. Rutile occurs as an inclusion within micas, whereas ilmenite occurs both as an inclusion and as individual disseminated grains. Where rutile and ilmenite are inclusions within mica, they are aligned along the cleavage.

5. Geochemistry

5.1. Major and trace elements

All of the granite types plot well within the peraluminous field on the A/NK vs. A/CNK [(Al₂O₃/(Na₂O+K₂) vs. Al₂O₃/(CaO+N₂O+K₂)] diagram (Figure 6a). A/CNK values are similar for the biotite, tourmaline and muscovite granites, averaging ~1.25. The topaz granites have a higher average A/CNK of 1.35. (Table 3).

In all major and trace element plots there is a broad geochemical continuum between G1 and G2 granites and G3 and G4 granites with G5 granites and aplites forming their own trends. G2 and G4 granites plot towards the higher SiO₂ values indicating their more evolved characteristics. Using both SiO₂ and tFe₂O₃ as differentiation indices, differing trends for the G1-G2, G3-G4 and G5 granites are observed. The “femic suite” of elements (Ti, Fe and Mg) and CaO all show negative trends with increasing SiO₂ but the G1-G2 and G3-G4 granites show subtle variations in gradient of the trends, relative to each other, whereas G5 granites show their own trend (e.g. Figure 6b). Na₂O increases with increasing SiO₂ in the G1-G2 and G3-G4 granites, showing similar gradients, whereas for G5, the trend varies from that of the other granites (Figure 6c). Plotting the differentiation indices K/Rb and Rb/Sr against tFe₂O₃ show slightly curved trends for G1-G2 and G3-G4 granites, with G5 granites plotting towards low K/Rb and high Rb/Sr due to high overall Rb (Figure 6d-e).

Zirconium, Th, Sr and Ba have positive correlations with Fe₂O₃ (e.g. Figure 6f). The majority of G1 and G3 granites show Zr concentrations over the 100 ppm zircon saturation threshold expected of a peraluminous melt at 750°C, implying source inheritance or high melting temperatures (Watson and Harrison, 1983). Barium vs. Rb shows a curved trend from high Ba / low Rb in G1 and G3 granites through G2 and G4 to G5 granites which have abundant Rb (Figure 6g). Classification of biotite, tourmaline and topaz granites using a Zr vs. Nb plot (Manning et al., 1996) can be replicated in this study, showing that the G1, G2 and G3 granites have a wide Zr range with little Nb change whereas the G4 granites have moderate Zr and Nb concentrations with G5 granites plotting towards high Nb but low Zr

(Figure 6h). The major and trace element geochemistry of the Cornubian granites has been fairly well established and this study is broadly in agreement with previous studies (e.g. Charoy, 1986; Stone, 1992; Manning et al., 1996; Stone, 2000; Chappell and Hine, 2006; Müller et al., 2006a) (Supplementary Table 2).

5.2. Rare Earth Elements (REE)

The G1 and G3 granites show similar light rare earth element (LREE) enriched patterns with negative Eu anomalies, although the G3 granites show a slightly stronger anomaly (0.31 ± 0.10) than G1 granites (0.38 ± 0.07) (Figure 7a,c). The most evolved G2 granites show stronger Eu anomalies (0.33 ± 0.10) and have lower total rare earth elements (Σ REE) than G1 granites (Figure 7b). The G4 granites show similar patterns to the G3 granites but have lower Σ REE and stronger negative Eu anomalies ($0.17 \pm 0.05 - 0.25 \pm 0.07$) (Figure 7d). G5 granites have lower Σ REE abundances than the biotite, muscovite and tourmaline granites and have flat profiles with heavy rare earth element enrichments and strong Eu anomalies (0.20 ± 0.05) (Figure 7e). G2 and G4 granites show slight Ce anomalies. Rare earth element patterns and Eu anomaly values in this study are consistent with previous studies (e.g. Chappell and Hine, 2006; Müller et al., 2006a).

6. Petrogenetic modelling

The trends shown on the major and trace element plots (Figure 6,7) could be due to one or more of the processes listed in the introduction such as fractional crystallisation, varying degrees of partial melting (e.g. Harris et al., 1995), source variation (e.g. Nabelek and Bartlett, 1999) and magma mixing (e.g. Patiño-Douce, 1999). Minerals such as plagioclase,

alkali feldspar and biotite can be involved in multiple processes such as partial melting and fractional crystallisation. Rubidium, Ba, and Sr all partition into micas and feldspars, rather than accessory minerals (e.g. Blundy and Wood, 1991) and are used here to model these processes. Rare earth elements partition into micas and feldspars also, but are often controlled by accessory minerals so care must be taken in using them for modelling (e.g. Bea, 1996). As REE-bearing minerals are dominantly locked within biotite in these samples, it is presumed that processes fractionating biotite also fractionate REE minerals. For the REE modelling, Pr, Ho and Tm were omitted due to limited partitioning data and Tb was omitted due to a lack of analyses. Muscovite and tourmaline are excluded from all models as they can have either late stage or subsolidus characteristics. However, muscovite is included in melting models as it is consumed in initial melting reactions. Partition coefficients used throughout this chapter are taken from studies of peraluminous melts and the batch melting and Rayleigh fractionation equations used for modelling (Eq. (A.1-2); Table A.1).

6.1. Source compositional characteristics

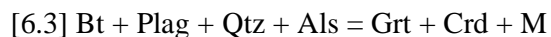
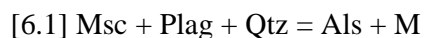
The source characteristics of the granites have been estimated using the plots of experimental data compiled by Patiño-Douce (1999). The G1 and G3 biotite granites plot within the greywacke field with some suggestion of mixing with a tholeiitic source (Figure 8). The G5 granites plot within the felsic pelite field, indicating a potentially distinctive source relative to the G1 and G3 granites (e.g. Manning and Hill, 1990; Stone, 1992).

Partial melting modelling was performed with Ba, Sr, Rb and REE for the G1-G2, G3-G4 and G5 granites using the modal mineral abundances for metagreywackes and metapelites of Nabelek and Bartlett (1999). Metagreywackes are distinguished from metapelites by their lower abundance of micas and higher proportion of plagioclase relative

to alkali feldspar. Since pre-Devonian basement is not exposed in SW England, it is not possible to identify a correlative high-grade greywacke-pelite source for major and trace element modelling of partial melting and differentiation. The greywacke sandstones of the upper plate-derived peri-Gondwanan Gramscatho Group were used as a compositional proxy (Floyd and Leveridge, 1987; Scott et al., 2003; Nance et al., 2015). The original source comprised 45% quartz, 35% plagioclase, 13% biotite, 3% garnet, 2% alkali feldspar, 1% muscovite and 1% aluminosilicates which lies within the compositional constraints for the Gramscatho Formation (Floyd and Leveridge, 1987) and greywacke material (e.g. Nabelek and Bartlett, 1999).

6.2. *Partial melting conditions*

The use of the zircon thermometry equation from Watson and Harrison (1983) indicates that the older G1 biotite granites formed at temperatures of 731-806°C with the younger G3 biotite granites forming at temperatures of 768-847°C (Table 3), consistent with the findings of Chappell and Hine (2006) and Drivenes et al (2016). There have been numerous experimental studies constraining melting reaction P-T conditions for pelites and greywackes (e.g. Huang and Wyllie, 1981; Patiño Douce and Johnston, 1991; Vielzeuf and Montel, 1994; Johnson et al., 2008). Partial melting of greywackes occurs through muscovite melting [6.1-6.2] followed by biotite melting at higher temperatures on a clockwise P-T-t path through incongruent melting reactions [6.3-6.4]:



Where: Msc = muscovite, Plag = plagioclase, Qtz = quartz, Als = aluminum silicates, Kfld = alkali feldspar, Bt = biotite, Grt = garnet, Crd = cordierite, Opx = orthopyroxene and M = melt.

As greywackes are typically muscovite deficient, the critical melt fraction (CMF), the minimum melt required for segregation, estimated to be >15% (Clemens and Vielzeuf, 1987), will not be reached. However, muscovite melting can be accompanied by minor biotite melting, increasing the CMF to a level at which melt can be extracted (Pickering and Johnston, 1998). Muscovite melting can also produce biotite from ferromagnesian components present within the muscovite (Patiño-Douce and Harris, 1998).

Charoy (1986) estimated that final crystallisation of the Carnmenellis Granite (G1) occurred at 650°C and 2-2.5 kbar with a water content of ~4 wt.%, although commented that the final pressure was probably lower. Pownall et al. (2012) determined that the Land's End Granite (G3-G4) was emplaced at 5-6 km depth (corresponding to 1.5 ± 1.0 kbar and 615 ± 50 °C) by P-T modelling of a cordierite-anthophyllite contact metamorphic assemblage. A previous estimate of the general conditions of batholith formation estimated a liquidus temperature of 720-770°C at 1.0-0.5 kbar (Chappell and Hine, 2006).

The high modal abundance of muscovite and accessory andalusite within the G1-G2 granites and a widespread occurrence of accessory cordierite within the G3 granites, allows them to be placed within specific zones on petrogenetic grids. Muscovite crystallises at lower temperatures and higher pressures relative to cordierite, which crystallises at higher temperatures and lower pressures (e.g. Huang and Wyllie, 1981; Monier and Robert, 1986; Clarke, 1995). The current mineral assemblage of the granites must therefore correlate to reactions involving muscovite and cordierite for G1 and G3 granites respectively (see also Charoy, 1986; Villaseca et al., 2008). The presence of F and B within the granite melts shifts the system minimum towards lower temperatures where andalusite and white mica become

stable (Pichavant and Manning, 1984). Taking these factors into account, the older G1 granites of the G1-G2 series are considered to have been generated by muscovite-dominated partial melting, within the temperature and pressure ranges for muscovite to be involved in melting / crystallisation reactions (Figure 9a); there was a minor contribution from biotite melting in order to achieve the CMF. The younger granites of the G3-G4 series are considered to have formed by biotite-dominated partial melting, at higher temperatures and lower pressures, within the lower pressure, higher temperature cordierite stability field (Figure 9b) (e.g. Clark, 1995). The cordierite stability field is consistent with source tourmaline melting, which occurs at 750-775°C at 3 kbar (Holtz and Johannes, 1991); there is increased tourmaline within the G3-G4 granites relative to G1-G2 granites.

6.3 Batch melting modelling

The samples representing the partial melt were the least geochemically evolved within the G1-G2 and G3-G4 granites (identified as those with highest femic components, REE, Ba and Sr and/or lowest Rb and SiO₂). Iterative trace element and REE modelling required up to 20% partial melting of a metagreywacke in order to produce melts with a composition approximating the most primitive G1 granites (Figure 10a-b) (Supplementary Table 3).

Melts approximating the composition of the most primitive G3 granites could only be adequately modelled if the source composition was first modified by: (i) removal of muscovite and alkali feldspar, (ii) increasing plagioclase from 35 to 42%, and (iii) decreasing garnet from 3 to 1%. Up to 30% partial melting of this modified source comprising 43% quartz, 42% plagioclase, 12% biotite, 1% garnet, 1% cordierite, 1% aluminosilicates and minor zircon, apatite and ilmenite generates primitive G3 granites (Figure 10c-d) (Supplementary Table 4). The decrease in the garnet abundance may not be entirely realistic

as garnet will undergo changes in HREE zoning that occurs at temperatures of muscovite melting (Harris et al., 1995) which will affect the distribution of HREE within the source. Therefore, modelling of HREE for the G3-G4 granites may be affected by source variations in garnet that would have been generated during muscovite-dominant melting.

6.4. Fractional crystallisation (mineral-melt separation)

Plotting the compositions of the least evolved major minerals against whole rock major element composition can indicate possible fractionating mineral assemblages (e.g. Tartèse and Boulvais, 2010). The least evolved mineral compositions are magnesium siderophyllite and calcic plagioclase for the G1-G2 trend and siderophyllite and calcic plagioclase for the G3-G4 trend. The evolution from G1 to G2 granites can be modelled by fractionation of an assemblage comprising alkali feldspar (25%), plagioclase (An_{25} , 54-46%) and biotite (19-21%) (Supplementary Figure 1a-b). The evolution from the G3 biotite granites to the G4 tourmaline granites can be modelled by fractionation of an assemblage comprising plagioclase (An_{25} , 20-25%), alkali feldspar (50%) and biotite (25-30%) (Supplementary Figure 1c-d).

Trace element modelling is consistent with major element behaviour. The evolution from least evolved G1 granite to most evolved G2 granite can be modelled for Ba, Sr and the REE by up to 30% fractionation of an assemblage comprising 23% alkali feldspar, 50% plagioclase (An_{25}), 20% biotite (magnesium siderophyllite), 4.6% garnet, 0.1% zircon, 0.8% apatite, 0.6% allanite, 0.2% ilmenite and 0.7% monazite (Figure 11a-b) (Supplementary Table 5). A differing trend is shown by the G3-G4 granite series. Up to 40% fractionation of an assemblage comprising 25% biotite (siderophyllite), 20% plagioclase (An_{25}), 50% alkali feldspar, 1.5% cordierite, 1% garnet, 0.4% ilmenite, 0.8% apatite, 0.2% zircon, 0.6% allanite

and 0.5% monazite is sufficient to account for the entire compositional variation (Figure 11c-d) (Supplementary Table 6). The deflection on the Ba vs. Sr plot (Figure 11c) away from the fractional crystallisation trend is likely to be a consequence of element mobility associated with hydrothermal fluid-rock reactions, also supported by scattering of the Rb/Sr ratio within evolved G4 granites (Figure 6e).

6.5. The G5 (topaz) granites

The melting models used for the G1-G2 and G3-G4 granites cannot explain the compositional characteristics of the G5 granites. Even very low degrees of partial melting of a metasedimentary source cannot result in a melt composition corresponding to the least evolved G5 granite. Derivation of the G5 granite by fractionation of G1 or G3 granites produces melts that are too low in LREE and HREE. Major element plots, particularly TiO_2 and Na_2O vs. SiO_2 (Figure 6b-c), do not support common fractionation trends for G1-G2, G3-G4 and G5 granites. The problematical petrogenetic relationship between G1, G3 and G5 granites was previously recognised by Manning and Hill (1990) and Stone (1992).

Partial melting of lower crustal residues following the extraction of the G1 granite melt, as proposed by Manning and Hill (1990), cannot be replicated by trace element models. Such a residue would comprise plagioclase, alkali feldspar, garnet, quartz and sillimanite and produces a melt with abundances of REE, Sr and Ba that are too high and a Rb abundance that is too low (Manning and Hill, 1990). Partial melting of earlier formed G1 granite (e.g. Stone, 1992) would also be an unviable process as it would produce a magma with a REE abundance that is too high. Barium and Sr would also be higher due to melting of feldspars and the Rb abundance of the G5 granites would not be attained.

Melting of biotite-rich assemblage (i.e. 70% biotite), as suggested by Stone (1992), does lower the Σ REE abundance but the addition of a MREE-bearing mineral such as apatite and a LREE-bearing mineral such as allanite is required to lower the modelled melts to REE abundances exhibited by the G5 granites. Partial melting of a biotite-rich source produces a melt with Sr, Ba and REE abundances consistent with the G5 granites (Figure 12a-b). A high level of apatite melting is not unreasonable given the high P_2O_5 of the G5 granites (>0.45 wt. % relative to ~0.2 wt. % for G1 / G3 granites). Apatite solubility is high in strongly peraluminous melts, such as the topaz granites which have A/CNK > 1.3 compared to the G1 and G3 granites of ~1.2 (Wolf and London, 1994). Strong feldspar and feric mineral fractionation, as suggested by Stone (1992), is supported by the new data from this study. Major element plots of the least evolved plagioclase (oligoclase) composition, biotite and ilmenite indicate that these minerals, particularly plagioclase, control evolution of G5 granite composition (Supplementary Figure 2).

The compositions of the G5 granites cannot be obtained by fractionation from G1-G2 or G3-G4 granites. Continuing the G1-G2 trend produces a melt with too low LREE and HREE abundances whereas further fractionation of the G3-G4 trend produces a melt with too low M-HREE. In both cases, modelled melts remain slightly LREE-enriched, which is not consistent with the flat REE profiles for G5 granites (Figure 12c-d) (Supplementary Table 7).

6.6. Role of mantle source and crustal assimilation

Microgranular mafic enclaves (MME) were observed in all of the G3 granites and are described in detail by Stimac et al. (1995) who tentatively suggested an origin by hybridisation of basaltic melts. Radiometric data indicate that lamprophyres, basalts and granites are contemporaneous (e.g. Thorpe, 1987; Edwards et al., 1997; Dupuis et al., 2015).

The presence of MME and contemporaneous mafic and ultramafic rocks in other granitic terrains has resulted in speculation about the potential for mixing and metal transfer between mafic and felsic melts (e.g. Chappell, 1996; Štemprok and Seifert, 2010).

On plots of granite, enclave, basalt and lamprophyre major element composition, Al, K, Na, and P show no continuation of trends from granites through MME to lamprophyres or basalts. MgO vs. SiO₂, TiO₂ vs. SiO₂ and Sr vs. SiO₂ plots show a broad continuum through all sample types, with deflections from a linear trend from the granites for the MME, basalts and lamprophyres (Figure 13a-c). CaO/Na₂O vs. Al₂O₃/TiO₂ shows a continuation through granites and MME, but not towards lamprophyre and basalt compositions (Figure 13d). Magma mixing would be expected to result in linear trends through all compositions.

Previous studies have suggested that the abundance of some metals (B, Sn) is due to assimilation of country rock mudstones during granite ascent rather than magmatic processes (e.g. Williamson et al., 2010). Strontium and Nd isotopes show the clear separation between the majority of the country rocks analysed and the granites (Darbyshire and Shepherd, 1994). The same study also concluded that assimilation of country rock material would lower the $\delta^{15}\text{N}$ values and raise the NH_4^+ and REE budget beyond those seen. As the geochemical modelling indicates that REE and trace element abundances can be achieved through partial melting and fractional crystallisation alone, crustal assimilation is not believed to be a major process in controlling granite compositions in SW England, at least for the major and trace elements in this study.

6.7. Hydrothermal overprinting

Samples from all granite types show evidence for post-emplacement subsolidus or hydrothermal alteration. Evidence for post-magmatic activity includes: crystallisation of

quartz-tourmaline orbicules in G3 granites (e.g. Drivenes et al., 2015), muscovite overgrowth on primary trioctahedral micas, scatter of Rb vs. SiO₂ towards higher SiO₂ values and increasing U with SiO₂, all characteristics of granites that have undergone modification by late-stage fluids (e.g. Haapala, 1997; Förster et al., 1999; Ballouard et al., 2015). Trends for P₂O₅, such as a negative correlation with CaO (the Pedrobernardo-type trend) and a positive correlation with Rb and Al₂O₃, are typical of peraluminous granites (Bea et al., 1992; Wolf and London, 1994). The Pedrobernardo trend is particularly important, as when the CaO content is low, such as in the most evolved granites in this study, Ca rather than P becomes limiting component of apatite, concentrating P within residual fluids (Bea et al., 1992). There is a strong correlation between P and the elements typically concentrated in residual fluids such as Rb and U, but a strong negative correlation between P and compatible elements (Ba, Sr) (Figure 14). The G3-G4 show stronger evidence for fluid-rock processes and the G4 granites in the north of the Land's End Granite may represent the magmatic precursors to magmatic-hydrothermal mineralisation in the region (Müller et al., 2006a).

7. Discussion

Field relations, geochemistry, mineralogy and mineral chemistry for the Cornubian granites clearly subdivide the plutons into five main groups. Two-mica (G1) and muscovite (G2) granites are represented by older plutons (Isles of Scilly, Carnmenellis, Bodmin, Cligga, Kit Hill, Hingston Down, Hemerdon). Younger plutons (Land's End, St. Austell and Dartmoor) dominantly comprise biotite (G3) and tourmaline (G4) granites, with rare occurrences of topaz (G5) granites within the Tregonning and St. Austell plutons. The peraluminous nature of the Cornubian Batholith, with coeval mafic ultrapotassic magmatism and presence of MME, is consistent with the post-collisional setting of Frost et al. (2001),

where influxes of mantle-derived magma induce crustal anatexis by dehydration melting reactions (section 6).

7.1. Petrogenesis of the Early Permian Cornubian Batholith

7.1.1. Tectonic controls on melting

The Cornubian Batholith occupies a lower plate position relative to the Variscan Rhenohercynian-Rheic suture. Its G1-G2 granites have similar characteristics to muscovite-bearing peraluminous granites (MPG) of Barbarin (1996) (see Table 1). However, unlike MPG, the oldest Cornubian granites (≥ 290 Ma) were emplaced > 65 Ma after initial Variscan collision in SW England at *c.* 360 Ma (Shail and Leveridge, 2009). Modest collisional crustal thickening, as evidenced by almost ubiquitous sub-greenschist facies regional metamorphism of the host rocks (Warr et al., 1991), would have raised lower crustal temperatures during the Carboniferous but, even if partial melting was initiated, the absence of felsic igneous rocks of this age do not suggest effective melt segregation. The low abundance of muscovite within a metagreywacke source would ensure that a critical melt fraction could not be achieved by muscovite melting alone.

The onset of generation and emplacement of the early G1-G2 granites at *c.* 293-292 Ma is contemporaneous with the first occurrence of mantle-derived lamprophyres and basalts across SW England (Edwards et al., 1997; Dupuis et al., 2015). Whilst the source region may have still been anomalously warm following convergence-related thickening, it was extensional exhumation of the lower plate and emplacement of mantle-derived melts that triggered the partial melting resulting in the MPG-like G1 and G2 granites. Mantle He signatures are present in sulphide mineralisation associated with the earliest through to latest

granites and support persistent devolatilisation of such mantle-derived melts (Shail et al., 2003).

The Cornubian G3-G4 granites are very similar to cordierite-bearing peraluminous granites (CPG) (Barbarin, 1996). Cordierite-bearing peraluminous granites exhibit a marked increase in biotite, cordierite and MME over G1-G2 (see Table 1). The transition to higher temperature ($>806^{\circ}\text{C}$) but lower pressure (<4 kbar) source melting to generate the G3-G4 granites is consistent with continued lower plate exhumation during regional extension. By the time the younger G3 biotite granites were emplaced (~ 280 Ma) the region had been undergoing post-Variscan extension for >20 Ma. Given minimum estimates of batholith thickness of 5-6 km (Taylor, 2007) and up to 50% partial melting of the lower-mid crust implied by our models, based on greywacke melt production data of Sawyer et al. (2011), the minimum thickness estimate of the lower-mid crustal melting zone is 12 km, although this can be reduced by lateral melt transport from outside the known surface crop of the batholith.

7.1.2. *Two-mica, muscovite, biotite and tourmaline granites (G1-G4)*

A greywacke source is consistent with the studies of Darbyshire and Shepherd (1994) and Chappell and Hine (2006). A greywacke rather than pelitic source is also consistent with the mineralogy and geochemistry of the exposed granites; a pelitic source would be expected to produce leucogranite with higher modal abundances of muscovite and limited occurrences of ferromagnesian minerals along with lower Sr and Ba but higher Rb (Pickering and Johnston, 1998). The source characteristics required for the most primitive G3 melts are consistent with a metagreywacke that had previously undergone melt extraction following muscovite-dominated partial melting (Harris et al., 1995; Nabelek and Bartlett, 1999).

Interpretations of the extent of the mantle contribution using enclave geochemistry can be problematic due to chemical exchange of elements between the granite melt and the enclave (e.g. Stimac et al., 1995). However, the trends on major and trace element plots (Figure 13) do suggest some mixing of a crustal melt with a mantle source, just not necessarily one represented by the geochemistry basalt or lamprophyres exposed within the study area. A mantle source or *extensive* mixing with magma from a mantle source is precluded at least at the current exposure levels. This is supported by Sr and Nd isotope data which imply mixing of a greywacke-type source with a minor mantle-derived component for G1 and G3 granites (e.g. Darbyshire and Shepherd, 1994) and melt inclusion analysis that do not suggest a mantle component within evolved G4 granites within the Land's End Granite (Müller et al., 2006b). Furthermore, the granites have $\delta^{18}\text{O}$ values of 10.8-13.2 ‰, interpreted as representing melting of argillaceous-rich metasediments (Sheppard, 1977), consistent with the geochemical findings of this study. It is widely accepted that only ferromagnesian mineral-poor peraluminous granites (leucogranites) are entirely crustal derived (e.g. Barbarin, 1996; Patiño-Douce, 1999).

The fractionating assemblages determined by this study are consistent with the observations of Stone (1992), Ward et al. (1992), Darbyshire and Shepherd (1994) and Müller et al. (2006a), that granite evolution was controlled by feldspars and biotite, along with biotite-hosted REE-bearing accessory minerals. The fractionating assemblage for the G3-G4 series is similar to that described by Ward et al. (1992), including the discrepancy between modelled and observed Eu. This variation could be attributed to variable partitioning of Eu within plagioclase which shows distinctive zoning with more calcic cores. The fractional crystallisation models are supported by variations in mineral chemistry. The decrease in the anorthite content of plagioclase, increase in the Li abundance within trioctahedral micas and tourmaline with a decrease in the femic components in both the G1-

G2 and G3-G4 granites is consistent with a fractionation model. This is common with granite suites elsewhere that have been affected by fractional crystallisation (Jung et al., 2000; Tartèse and Boulvais, 2010; Neiva et al., 2011; Ballouard et al., 2015). Given the strong correlation in SW England between geochemically similar granites (G1/G2 vs. G3/G4) and age, source heterogeneity (e.g. Clemens, 2003) is not invoked as a major control on granite variation.

7.1.3. Topaz (G5) granites

It is accepted that the high-F abundances of the G5 granites could be achieved by fractionation, as demonstrated by models for rare metal granites in France and Germany (e.g. Raimbault et al., 1995; Breiter et al., 2005). However, in these models volatile separation forms B-depleted, and therefore tourmaline depleted rocks, but the SW England G5 granites contain tourmaline. The G3-G4 granite trend displays a marked increase in B, with abundant tourmaline in G4 granites (Table 1). Continued fractionation should enrich B further to the point of volatile separation, but previous data show a B_2O_3 abundance of 0.17-0.36% in G4 granites and of 0.1% in G5 granites (Manning and Hill, 1990).

Additionally, the only ages for the G5 granites are low precision Rb-Sr dates that place them between G1 and G3 granites (Darbyshire and Shepherd, 1987). As the G1 and G2 granites are not strongly enriched in Li and F, as indicated by mineral compositions, and P, it is unclear how these elements would be enriched within the G5 granites. Given the lack of exposures of another granite type that appears petrogenetically linked with the G5 granites, it is difficult to fully ascertain the processes controlling their petrogenesis. What is clear however, is that whilst G3-G4 granites have higher Li and F, indicated by mineral composition, and P, they are always intimately linked in the field, both containing MME, and

with gradational contacts. G5 granites do not display these characteristics, forming discrete intrusions. In Spain, the Belvís de Monroy leucogranite, is a reverse zoned pluton with evolved Li- and P-rich units. The most evolved leucogranites are interpreted as evolving in a deep chamber, from a source compositionally similar to other less evolved exposed granites, rather than evolving through fractionation of the exposed, less evolved granites, similar to the G3-G4 and G5 granites. The potential to reach shallow emplacement levels is aided by high concentrations of volatile and fluxing components (Merino et al., 2013).

It is proposed by Christiansen et al. (1988) and Cuney and Barbey (2014) that granulite facies metamorphism of a crustal source will liberate Li, P, F and HFSE from source mica with these elements partitioning into a fluid. This fluid is then transported, through shear zones and faults, to higher levels in the crust where melting is induced. High concentrations of elements such as F, P, Li and B decrease the solidus temperature and viscosity of any melt formed so lower degrees of partial melting are required before granitic melts are extracted. Manning and Hill (1990) inferred that the occurrence of the G5 granites in SW England is most likely controlled by basic magmas and granulite-facies rocks, with the fluxing elements potentially coming from the basic magma. Therefore, the G5 granites are tentatively interpreted to result from flux-induced melting of biotite-rich restite in the lower crust with strong feldspar fractionation; as a biotite-rich source is suggested by modelling (Supplementary Table 7).

The G5 granites of the Cornubian Batholith were used to define the “high-P” subtype of topaz granites by Taylor (1992), distinguished from the “low-P” subtype by very low REE, Y and Th, $P_2O_5 > 0.4$ wt.% and a relation to “S-type” peraluminous granites (Bonin, 2007). In contrast, the “low-P” subtype have high REE, Y, Th, affinities with metaluminous (to weakly peraluminous) granites and characteristics typical of A-type granites (e.g. Breiter, 2012). Isotopic data suggest large mantle inputs into A-type granites and there are no

experimental data that support a solely crustal derivation (Bonin, 2007). The topaz granites of the Cornubian Batholith do not exhibit geochemical or isotopic characteristics typical of A-type topaz granites associated with anorogenic intra-cratonic settings.

7.3. Comparison with petrogenetic models for other peraluminous granites

The Cornubian granites have similarities with other European Variscan granites. The Central Iberian Zone (CIZ) in Portugal and Spain shows the strongest correlation with the Cornubian G1-G2 and G3-G4 granites. In the CIZ there are late-stage two-mica and muscovite-bearing granites, derived from partial melting of sedimentary sources and linked through fractionation, that are associated with mineralisation (Carvalho et al., 2012; Teixeira et al., 2012). Additionally, intrusion of mantle-derived melts aided lower crustal partial melting and there was some mixing with a dominantly sedimentary-derived melts (Neiva et al., 2011). It is suggested by Romer and Kroner (2016) that Sn-W mineralisation, and therefore the granites from which this mineralisation is sourced, form from similar source rocks in SW England and Portugal (the “Cornwall type” model). Processes such as post-collisional extension, heat through upwelling mantle melts, changing P/T conditions of melting and fractionation are common to the RHZ and CIZ. The geochemical and mineralogical variation within the Erzgebirge / Krušné hory, within the Saxo-Thuringian Zone of the Variscan Orogen, is interpreted as melting of a heterogeneous metasedimentary and metaigneous source to produce a range of compositions characteristic of I-, S- and A-type granites (e.g. Breiter, 2012). The Cornubian Batholith does not show such variation.

The G5 (topaz) granites of the Cornubian Batholith exhibit many geochemical and mineralogical similarities with rare metal granites (RMG) (e.g. Raimbault et al., 1995; Černý et al., 2005). Peraluminous RMG are characterised by extreme enrichment of Li, B, F, P, and

Rb, extremely low REE and Zr, and a mineralogy dominated by Li-rich micas such as lepidolite and plagioclase that is almost pure albite. There are several global analogues for such topaz granites including the Variscan Beauvoir Granite, Massif Central, France, (Cuney and Barbey, 2014) and the Variscan Podlesí Stock, Czech Republic (e.g. Breiter et al., 1997).

8. Conclusions

1. The Early Permian Cornubian Batholith is a composite peraluminous batholith that was generated and emplaced over 20 Ma in the lower plate of the Rheohercynian / Rheic suture during post-Variscan extension. Lamprophyres and basalts are coeval with granite magmatism.
2. The exposed granites can be classified as G1 (two-mica), G2 (muscovite), G3 (biotite), G4 (tourmaline) and G5 (topaz). Each has a distinctive mineralogy and exhibits variable size and abundance of alkali feldspar phenocrysts and groundmass grainsize.
3. G1 (two-mica) granites are the oldest granites and formed through muscovite and minor biotite dehydration melting of a greywacke source at moderate temperatures and pressures (731-806°C, >5 kbar). Melting was driven by the emplacement of mantle-derived mafic igneous rocks into the lower crust.
4. G3 (biotite) granites are younger and formed by biotite-dominated melting of a similar source under slightly higher temperature but decreased pressure conditions (768-847°C, <4 kbar) consistent with the ongoing emplacement of mantle-derived melts and crustal melting during lower plate exhumation.
5. Trends shown by major and trace element mineral chemistry, such as decreasing Fe, Ti and Mg with increasing Si and increasing Rb coupled with decreasing Mg and Li contents in trioctahedral micas, decreasing Mg in tourmaline and decreasing anorthite content in plagioclase support fractionation as the dominant control linking G1-G2 and G3-G4 granites.

Fractionation was dominated by biotite, feldspars, zircon, ilmenite and REE-bearing accessory minerals. Both G1-G2 and G3-G4 granites require fractionation of 15-30% to account for compositional ranges.

6. Mafic microgranular enclaves (MME) are widespread in G3 and G4. However, there is limited or no geochemical evidence of substantial mixing between mantle- and crustally-derived magmas. Major and trace element plots of granites, MME and coeval lamprophyres and basalts do not suggest that the lamprophyres and basalts represent mixing end-members. The G3 granites appear to show an increased, but still minor, mantle-derived component.

7. The G5 (topaz) granites are compositionally distinct and cannot be formed by fractionation of biotite or tourmaline granite magmas. An origin through melting of the biotite-rich restite remaining after extraction of G3 (biotite) granite magmas is favoured. Such melting was induced by fluids containing a high abundance of F, Li, P and HFSE derived from granulite facies dehydration melting of the lower crust, during emplacement of mantle-derived melts.

8. G1-G2 granites are similar to post-collisional peraluminous granites described within the Central Iberian Zone. G3-G4 granites, with cordierite and forming through high-temperature, low-pressure melting are consistent with cordierite-bearing peraluminous granites, described by Barbarin (1996), formed through melting induced by injection of mafic rocks into the crust. G5 granites are most similar to descriptions of rare metal granites (e.g. Beauvoir, Massif Central) and do not show geochemical characteristics typical of A-type topaz granites formed within anorogenic settings.

Acknowledgments

This study was supported by the European Regional Development Fund and European Social Fund as part of the convergence funding for Cornwall and the Isles of Scilly (Combined Universities in Cornwall project number 11200NCO5), supporting a PhD for BS, and the European Union (Horizon 2020 project 641650 FAME). The Natural History Museum, London, UK are thanked for the loan of samples. We thank Richard Scrivener and Nicholas LeBoutillier for help with sampling. Steve Pendray, Sharon Uren and Joe Pickles assisted with the sample preparation and analysis. Axel Müller and Karel Breiter are thanked for discussions about topaz granites. We gratefully acknowledge Romain Tartèse and an anonymous reviewer for their constructive comments which helped to improve the manuscript.

Appendices

Eqs. 1-2 Trace element modelling equations and partition coefficients

After Shaw (1970):

[Eq. 1] Batch melting: $C_L / C_O = 1 / [D (1-F) + F]$

[Eq. 2] Rayleigh fractionation: $C_L / C_o = F^{(D-1)}$

where:

C_L = Weight concentration of a trace element in the melt

C_O = Weight concentration of a trace element in the source

D = Bulk distribution coefficient for residual solids (batch melting) or the fractionating assemblage (Rayleigh fractionation)

F = Weight fraction of melt produced (batch melting) or the fraction of melt remaining (Rayleigh fractionation)

	Qtz	Kfld	Plag	Bt	Msc	Grt	Crd	Zrc	Ap	Ilm	Mon
Rb	0.012	1.75	0.09	1.84	1.51	0.009	0.08	0*	0.001	0*	0*
Sr	0*	13.98	6.80	0.38	0.52	0.015	0.12	0*	4.3	0*	0.5**
Ba	0.015	12.59	0.63	15.67	5.62	0.017	0.02	0*	0.12	0*	0.1**
Ref	1	2	1	3	1	4	5	-	10	-	8
La	0.02	0.08	0.38	0.06	0*	0.39	0.06	16.90	14.50	1.31	298
Ce	0.01	0.04	0.27	0.05	0*	0.69	0.07	16.75	21.10	1.19	277
Nd	0.02	0.04	0.20	0.08	0*	0.60	0.09	13.30	32.80	0.96	290
Sm	0.01	0.03	0.17	0.06	0*	2.04	0.10	14.40	46.00	0.68	217
Eu	0.06	4.45	4.45	0.05	0*	0.52	0.01	16.00	25.50	0.40	114
Gd	-	-	0.13	0.10	0*	6.98	0.29	12.00	43.90	-	175
Dy	0.02	0.06	0.11	0.17	0*	28.60	0.99	101.50	34.80	0.37	83
Er	-	0.03	0.08	0.22	0*	25.00	3.03	135.00	22.70	-	44
Yb	0.02	0.03	0.09	0.12	0*	43.48	1.77	527.00	15.40	0.55	18
Lu	0.01	0.03	0.09	0.20	0*	39.78	4.43	641.50	13.80	0.74	13
Ref	1	1,6	1	5		9	5	6	7	6	8

1 – Nash and Crecraft (1985); 2 – Icenhower and London (1996); 3 – Icenhower and London (1995); 4 – Arth (1976); 5 – Bea et al. (1994); 6 – Mahood and Hildreth (1983); 7 – Fujimaki (1986); 8 – Stepanov et al. (2012); 9 – Irving and Frey (1978) ; 10 – Prowatke and Klemme (2006). *Estimated as 0 (i.e. less than trace amounts); **Stated as less than unity (0.5) or below detection (0.1).

Appendix references

Arth, J.G., 1976. Behaviour of trace elements during magmatic processes - a summary of theoretical models and their applications. *Journal of Research of the US Geological Survey* 4, 41-47.
 Bea, F., Pereira, M.D., Stroch, A., 1994. Mineral / leucosome trace-element partitioning in a peraluminous migmatite (a laser ablation-ICP-MS study). *Chemical Geology* 117, 291-312.
 Fujimaki, H., 1986. Partition coefficients of Hf, Zr and REE between zircon, apatite and liquid. *Contributions to Mineralogy and Petrology* 94, 42-45.

- Icenhower, J., London, D., 1995. An experimental study of element partitioning among biotite, muscovite, and coexisting peraluminous silicic melt at 200 MPa (H₂O). *American Mineralogist* 80, 1229-1251.
- Icenhower, J., London, D., 1996. Experimental partitioning of Rb, Cs, Sr, and Ba between alkali feldspar and peraluminous melt. *American Mineralogist* 81, 719-734.
- Irving, A.J., Frey, F.A., 1978. Distribution of trace elements between garnet megacrysts and host volcanic liquids of kimberlitic to rhyolitic compositions. *Geochimica et Cosmochimica Acta* 42, 771-787.
- Mahood, G., Hildreth, W., 1983. Large partition coefficients for trace elements in high-silica rhyolites. *Geochimica et Cosmochimica Acta* 47, 11-30
- Nash, W.P., Crecraft, H.R., 1985. Partition coefficients for trace elements in silicic magmas. *Geochimica et Cosmochimica Acta* 49, 2309-2322.
- Prowatke, S., Klemme, S., 2006. Trace element partitioning between apatite and silicate melts. *Geochimica et Cosmochimica Acta* 70, 4513-4527.
- Shaw, D.M. 190. Trace element fractionation during anatexis. *Geochimica et Cosmochimica Acta* 34, 237-243.
- Stepanov, A.S., Hermann, J., Rubatto, D., Rapp, R.P., 2012. Experimental study of monazite/melt partitioning with implications for the REE, Th and U geochemistry of crustal rocks. *Chemical Geology* 300–301, 200-220.

Figures

Figure 1. Geological map of SW England showing the principal mineralogical and textural variations in the Cornubian Batholith. It combines a mineralogical classification into two-mica, muscovite, biotite, tourmaline and topaz granites with a textural scheme based primarily on mean matrix grain-size and the size and abundance of alkali feldspar phenocrysts. Compiled from Ghosh (1927), Exley and Stone (1982), Dangerfield and Hawkes (1981), Manning et al. (1996), (Selwood et al., 1998); Müller et al. (2006a) and British Geological Survey data (Geological Map Data © NERC 2016) with additional observations from this study.

Figure 2. Examples of the mineralogical and textural variations within the granites of the Cornubian Batholith: **a** – Coarse-grained, porphyritic G1a biotite-muscovite granite from Holman's Test Mine, Carnmenellis Granite. **b** – Coarse-grained porphyritic G2 muscovite granite from Kit Hill. **c** – Coarse-grained porphyritic G3 biotite granite from Lamorna,

Land's End Granite. **d** – Globular quartz G4 tourmaline granite from Karlake Pit, St. Austell Granite. **e** – Equigranular G5 topaz granite from Goonvean, St. Austell Granite.

Figure 3. Examples of internal contacts, granite fabrics and enclaves within the Cornubian Batholith. **A** – Sharp contact between G3a and G3d biotite granites near Porth Gwarra, Land's End Granite. **b** – Lobate enclave of G3d biotite granite in G3c biotite granite, Helman Tor, Dartmoor Granite. **c** – Abundant aligned alkali feldspar phenocrysts in G3a biotite granite at Nanjizal, Land's End Granite. **d** – Non-igneous enclave (metasedimentary rock) in G3a biotite granite, Porthledden, Land's End Granite. **e** – Mafic microgranular enclave (MME) and tourmaline cluster in G3a biotite granite, Dartmoor Granite.

Figure 4. Microscopic features of major and accessory minerals within the Cornubian Batholith. **a** – Magnesium siderophyllite biotite mica in G3a granite with numerous inclusions and associated metamictisation of the host grain. **b** – Zinnwaldite mica and topaz within G5 topaz granite, Tregonning Pluton. **c** - Abundant muscovite in G2 granite, Castle-an-Dinas, Land's End Granite. **d** – Zoned inclusions of quartz and plagioclase in an alkali feldspar (Kfs) phenocryst from the Isles of Scilly Granite (G1a). **e** – Tourmaline in a G1a granite from the Carnmenellis pluton. **f** – Cordierite with sixling twinning in G3a biotite granite, Land's End Pluton.

Figure 5. Selected diagrams showing mineral chemistry characteristics of the Cornubian Batholith **a** - Trioctahedral and dioctahedral mica compositions plotted on the classification diagram of Tischendorf et al. (1997). There is a chemical continuum shown by G1-G2 and G3-G4 granites from magnesian siderophyllite to zinnwaldite. **b.** - Ternary plot of plagioclase

compositions indicating an increasing albite component in the more evolved G2, G4 and G5 granites.

Figure 6. Classification, major and trace element plots for the G1-G5 granites of the Cornubian Batholith. **a** – A/NK vs. A/CNK plot displaying the peraluminous nature of the Cornubian granites. **b** – TiO₂ vs. SiO₂ showing a negative correlation for G1-G5 granites, with varying gradients for G1-G2, G3-G4 and G5 granites. **c** – Na₂O vs. SiO₂ showing positive correlations with various gradients for all granites. **d** – K/Rb vs. Fe₂O₃ showing a positive correlation, with some scatter, for G1-G4 granites. G5 granites plot towards low K/Rb due to strong Rb enrichment. **e** – Rb/Sr vs. Fe₂O₃ showing a curvilinear trend for G1-G2 and G3-G4 granites with upward scatter in Rb/Sr attributable to secondary Rb-enrichment. **f** – Positive correlation for Zr (ppm) vs. Fe₂O₃ (wt. %); the dashed line indicates Zr saturation in peraluminous melts (Watson and Harrison, 1983). **g** – Ba vs. Rb (ppm) displaying a curvilinear trend for all granites. **h** - Nb vs. Zr plot, modified after Manning et al. (1996). G1 and G3 granites plot towards higher Zr, lower Nb, G2 have decreased Zr, G4 granites show decreased Zr and increased Nb whereas G5 granites are Nb enriched and Zr depleted

Figure 7. Chondrite normalised REE plots for G1-G5 Cornubian granites. Lines show mean data, shaded areas displays all data. Data normalised using the values of McDonough and Sun (1995). There is an overall REE decrease and stronger Eu anomaly from G1-G2 granites and within the G3-G4 fractionating series. G5 granites show distinctive flat patterns with strong Eu anomalies. Figure 7e shows the mean REE data for each granite type, displaying the decrease in Σ REE from G1-G2 and G3-G4, with stronger Eu anomalies in G2, G4 and G5.

Figure 8. Compositions of G1, G3 and G5 granites of the Cornubian Batholith compared to the compositional ranges of experimental metasediment derived melts. Modified from Patiño-Douce (1999). The G1 and G3 granites plot within the greywacke field, showing some overlap with the mafic pelite field. G3 granites show suggestion of hybridisation with a tholeiitic melt, but this is not extensive. G5 granites plot within the felsic pelite field indicating their unique characteristics.

Figure 9. Pressure-temperature diagrams showing estimated conditions of anatexis (black stars) for **a** - Older G1 granites that form the G1-G2 fractionation series within the zone where muscovite is involved in melting reactions (shaded grey) and **b** - Younger G3 granites that form the G3-G4 fractionation series, within the zone where cordierite is involved in melting reactions (shaded grey). The light grey circle represents the estimated conditions of anatexis of Charoy (1986) for the Carnmenellis Granite (G1). The dark grey circle represents the conditions of emplacement of the Land's End Granite (G3) (Pownall et al., 2012). The displacement of the system minimum on addition of 2% B₂O₃ and 2% F is shown by the grey lines (after Pichavant and Manning, 1984). Abbreviations: Ab – albite; And – andalusite; As – aluminosilicates; Bt – biotite; Crd – cordierite; Grt – garnet; L – liquid; Kfld – alkali feldspar; Ky – kyanite; Opx – orthopyroxene; Sil – sillimanite; V – vapour; Redrawn after Spear et al. (1999).

Figure 10. Batch melting trace element and REE models of a greywacke source to produce **a-b** - G1 biotite granite and **c-d** - G3 biotite granite. REE data are chondrite normalised using the values of McDonough and Sun (1995). The least evolved G1 and G3 granites were selected for modelling. For G1 granites, 20% partial melting of a greywacke source produces

a melt with similar trace element characteristics the granites. For G3, 30% partial melting of a muscovite-depleted greywacke source is required.

Figure 11. Fractional crystallisation trace element and REE models for fractionation of the assemblage described in text from the most to the least evolved granites in the **a-b** G1-G2 granite series and **c-d** G3-G4 granite series. F is the weight fraction of melt remaining. REE patterns chondrite normalised using the values of McDonough and Sun (1995). For G1-G2 granites, the range of compositions can be sufficiently accounted for using the models discussed in text. For G3-G4 granites, there is a deflection from the modelled trend for the most evolved G4 granites, possibly due to fluid involvement.

Figure 12. **a** Trace element and **b** REE model of partial melting ($F=0.2$) of biotite-rich restite to form G5 granites. Substantial feldspar fractionation would be required or preferential partitioning of Eu into a fluid would be required to achieve the Eu anomaly observed in the G5 granites. Continued fractionation of the **c** G1-G2 granites and **d** G3-G4 granites would not produce a residual melt corresponding to that of the G5 granites. REE pattern chondrite normalised using the values of McDonough and Sun (1995).

Figure 13. Major element variation diagrams for granites, MME, lamprophyres and basalts, with the regression lines for G1 and G3 granites shown. The trend for G5 granites is not shown as there are too few data **a.** SiO_2 vs. MgO. The G1 regression line lies away from the MME trend whereas for G3 granites, the trend continues through MME, but mixing with the basalts is inconclusive. **b.** SiO_2 vs. MgO, showing a similar trend to MgO, although MME lie away from the G3 trend. **c.** SiO_2 vs. Sr. Positive correlation between G1 and MME, but not G3 and MME. Basalt compositions lie towards the end of the G1-MME trend, but

lamprophyres scatter upwards. **d.** $\text{Al}_2\text{O}_3/\text{TiO}_2$ vs. $\text{CaO}/\text{Na}_2\text{O}$ plot of Sylvester (1998). No continuation of the trend from G1 and G3 through MME, but not basalts and lamprophyres. There is no evidence of extensive mixing of mantle and crustal melts. MME compositions from Stimac et al. (1995) and basalts and lamprophyre compositions from Fortey (1992) respectively.

Figure 14. Correlations between P_2O_5 and **a** Rb (ppm) and **b** Sr (ppm). Rb is typically concentrated in residual fluids during granite evolution and there is a strong correlation between P and Rb but a strong negative correlation between P and Sr, which is incompatible in fluids.

Tables

Table 1. Summary of G1-G5 granite types with key macroscopic features, major and accessory mineralogy, age, occurrence, enclaves and other features.

Table 2. Mean microprobe data for plagioclase (core and rim) and orthoclase across different granite types.

Table 3. Mean geochemical data for G1-G5 granites. Major elements in wt. %, trace and rare earth elements in ppm. All data provided in Supplementary Table 2.

References cited

- Awad, N.T., Merefield, J.R., Scrivener, R.C., Stone, M., 1996. Geochemistry and petrogenesis of volcanic clasts in the Permian breccias around Exeter. *Journal of the Geological Society, London* 153, 669-672.
- Ballouard, C., Boulvais, P., Poujol, M., Gapais, D., Yamato, P., Tartèse, R., Cuney, M., 2015. Tectonic record, magmatic history and hydrothermal alteration in the Hercynian Guérande leucogranite, Armorican Massif, France. *Lithos*, 220-223, 1-22.
- Barbarin, B., 1996. Genesis of two main types of peraluminous granitoids. *Geology* 24, 295-298.
- Bea, F., 1996. Residence of REE, Y, Th and U in Granites and Crustal Protoliths; Implications for the Chemistry of Crustal Melts. *Journal of Petrology* 37, 521-552.
- Bea, F., Fershtater, G., Corretgé, L.G., 1992. The geochemistry of phosphorus in granite rocks and the effect of aluminium. *Lithos* 29, 43-56.
- Blundy, J.D., Wood, B.J., 1991. Crystal-chemical controls on the partitioning of Sr and Ba between plagioclase, feldspar, silicate melts and hydrothermal solutions. *Geochimica et Cosmochimica Acta* 55, 193-209.
- Bonin, B., 2007. A-type granites and related rocks: Evolution of a concept, problems and prospects. *Lithos* 97, 1-29.
- Bonin, B., Azzouni-Sekkal, A., Bussy, F., Ferrag, S., 1998. Alkali-calcic and alkaline post-orogenic (PO) granite magmatism: petrologic constraints and geodynamic settings. *Lithos* 45, 45-70.
- Bott, M.H.P., Day, A.A., Masson-Smith, D., 1958. The geological interpretation of gravity and magnetic surveys in Devon and Cornwall. *Philosophical Transactions of the Royal Society of London. Series A, Mathematical and Physical Sciences* 251, 161-191.
- Bouchez, J.L., Nguema, T.M.M., Esteban, L., Siqueira, R., Scrivener, R.C., 2006. The tourmaline-bearing granite pluton of Bodmin (Cornwall, UK): magnetic fabric study and regional inference. *Journal of the Geological Society* 163, 607-616.
- Breiter, K., 2012. Nearly contemporaneous evolution of the A- and S-type fractionated granites in the Krušné hory / Erzgebirge Mts., Central Europe. *Lithos* 151, 105-121.
- Breiter, K., Müller, A., Leichmann, J., Gabasova, A., 2005. Textural and chemical evolution of a fractionated granitic system: the Podlesi stock, Czech Republic. *Lithos* 80, 323-345.
- Carvalho, P.C.S., Neiva, A.M.R., Silva, M.M.V.G., Corfu, F., 2012. A unique sequential melting mechanism for the generation of anatectic granitic rocks from the Penafiel area, northern Portugal. *Lithos* 155, 110-124.
- Černý, P., Belvin, P.L., Cuney, M., London, D., 2005. Granite-related ore deposits. *Economic Geology* 100th Anniversary Volume, 337-370.
- Chappell, B.W., 1996. Magma mixing and the production of compositional variation within granite suites: Evidence from the granites of southeastern Australia. *Journal of Petrology* 37, 449-470.
- Chappell, B.W., Hine, R., 2006. The Cornubian Batholith: an example of magmatic fractionation on a crustal scale. *Resource Geology* 56, 203-244.
- Chappell, B.W., White, A.J.R., Wyborn, D., 1987. The importance of source material (restitute) in granite petrogenesis. *Journal of Petrology* 28, 1111-1138.
- Charoy, B., 1986. The genesis of the Cornubian Batholith (South-West England): the example of the Carnmenellis Pluton. *Journal of Petrology* 27, 571-604.
- Chesley, J.T., Halliday, A.N., Snee, L.W., Mezger, K., Shepherd, T.J., Scrivener, R.C., 1993. Thermochronology of the Cornubian Batholith in southwest England: Implications for pluton emplacement and protracted hydrothermal mineralisation. *Geochimica et Cosmochimica Acta* 57, 1817-1835.
- Christiansen, E.H., Stuckless, J.S., Funkhouser, M.J., Howe, K.A., 1988. Petrogenesis of rare-metal granites from depleted sources - an example from the Cenozoic of western Utah, USA, in: Taylor,

- R.P., Strong, D.F. (Eds.), Special Volume 39: Recent advances in the geology of granite-related mineral deposits. Canadian Institute of Mining and Metallurgy, Canada, pp. 307-321.
- Clark, A.H., Chen, Y., Farrar, E., B., N., 1994. Refinement of the time-space relationships of intrusion and hydrothermal activity in the Cornubian Batholith [Abstract only]. Proceedings of the Ussher Society, 345.
- Clarke, D.B., 1995. Cordierite in felsic igneous rocks: a synthesis. Mineralogical Magazine 59, 311-325.
- Clemens, J.D., 2003. S-type granitic magmas - petrogenetic issues, models and evidence. Earth Science Reviews 61, 1-18.
- Clemens, J.D., Vielzeuf, D., 1987. Constraints on melting and magma production in the crust. Earth and Planetary Science Letters 86, 287-306.
- Cuney, M., Barbey, P., 2014. Uranium, rare metals and granulite-facies metamorphism. Geoscience Frontiers, 1-17.
- Dangerfield, J., Hawkes, J.R., 1981. The Variscan granites of south-west England: additional information. Proceedings of the Ussher Society 5, 116-120.
- Darbyshire, D.P.F., Shepherd, T.J., 1987. Chronology of magmatism in souther-west England: the minor intrusions. Proceedings of the Ussher Society 6, 431-438.
- Darbyshire, D.P.F., Shepherd, T.J., 1994. Nd and Sr isotope constraints of the origin of the Cornubian Batholith, SW England. Journal of the Geological Society 151, 795-802.
- DePaolo, D.J., 1981. Trace element and isotopic effects of combined wallrock assimilation and fractional crystallisation. Earth and Planetary Science Letters 53, 189-202.
- Drivenes, K., Larsen, R., Müller, A., Sørensen, B., Wiedenbeck, M., Raanes, M., 2015. Late-magmatic immiscibility during batholith formation: assessment of B isotopes and trace elements in tourmaline from the Land's End granite, SW England. Contributions to Mineralogy and Petrology 169, 1-27.
- Drivenes, K., Larsen, R.B., Müller, A., Sørensen, B.E., 2016. Crystallization and uplift path of late Variscan granites evidenced by quartz chemistry and fluid inclusions: Example from the Land's End granite, SW England. Lithos 252, 57-75.
- Dupuis, N.E., Braid, J.A., Murphy, J.B., Shail, R.K., Archibald, D.A., Nance, R.D., 2015. $^{40}\text{Ar}/^{39}\text{Ar}$ phlogopite geochronology of lamprophyre dykes in Cornwall, UK: new age constraints on Early Permian post-collisional magmatism in the Rhenohercynian Zone, SW England. Journal of the Geological Society.
- Edwards, R.A., Warrington, G., Scrivener, R.C., Jones, N.S., Haslam, H.W., Ault, L., 1997. The Exeter Group, south Devon, England: a contribution to the early post-Variscan stratigraphy of northwest Europe. Geological Magazine 134, 177-197.
- Erdmann, S., Jamieson, R.A., Macdonald, M.A., 2009. Evaluating the origin of garnet, cordierite and biotite in granitic rocks: a case study from the South Mountain Batholith, Nova Scotia. Journal of Petrology 50, 1477-1503.
- Exley, C.S., Stone, M., 1964. The granitic rocks of south-west England, in: Hosking, K.F.G., Shrimpton, G.J. (Eds.), Present views of some aspects of the geology of Cornwall and Devon. Royal Geological Society of Cornwall, Penzance, pp. 131-184.
- Exley, C.S., Stone, M., 1982. Hercynian intrusive rocks, in: Sutherland, D.S. (Ed.), Igneous rocks of the British Isles. John Wiley & Sons, Chichester, pp. 287-320.
- Floyd, P.A., Leveridge, B.E., 1987. Tectonic environment of the Devonian Gramscatho basin, south Cornwall: framework mode and geochemical evidence from turbiditic sandstones. Journal of the Geological Society 144, 531-542.
- Förster, H.-J., Tischendorf, G., Trumbull, R.B., Gottesmann, B., 1999. Late-collisional granites in the Variscan Erzgebirge, Germany. Journal of Petrology 40, 1613-1645.
- Fortey, N.J., 1992. The Exeter Volcanic Rocks: Geochemistry. British Geological Survey Technical Report WG/92/7.
- Franke, W., 2000. The mid-European segment of the Variscides: tectonostratigraphic units, terrane boundaries and plate tectonic evolution. Geological Society London Special Publications 179, 35-61.

- Frost, B.R., Barnes, C.G., Collins, W.J., Arculus, R.J., Ellis, D.J., Frost, C.D., 2001. A Geochemical Classification for Granitic Rocks. *Journal of Petrology* 42, 2033-2048.
- Ghosh, P.K., 1927. Petrology of the Bodmin Moor Granite (eastern part), Cornwall. *Mineralogical Magazine* 21, 285-309.
- Haapala, I., 1997. Magmatic and postmagmatic processes in tin-mineralized granites: Topaz-bearing leucogranite in the Eurajoki Rapakivi Granite Stock, Finland. *Journal of Petrology* 38, 1645-1659.
- Harris, N., Ayres, M., Massey, J., 1995. Geochemistry of granitic melts produced during the incongruent melting of muscovite: implications for extraction of Himalayan leucogranite magmas. *Journal of Geophysical Research* 100, 15767-15777.
- Henderson, C.M.B., Martin, J.S., 1989. Compositional relations in Li-micas from SW England and France: an ion- and electron-microprobe study. *Mineralogical Magazine* 53, 427-449.
- Holtz, F., Johannes, W., 1991. Effect of tourmaline on melt fraction and composition of first melts in quartzofeldspathic gneiss. *European Journal of Mineralogy* 3, 527-536.
- Huang, W.L., Wyllie, P.J., 1981. Phase relationships of S-type granite with H₂O to 35 kbar: Muscovite granite from Harney Peak, South Dakota. *Journal of Geophysical Research* 86, 10515-10529.
- Johnson, T.E., White, R.W., Powell, R., 2008. Partial melting of metagreywacke: a calculated mineral equilibria study. *Journal of Metamorphic Geology* 26, 837-853.
- Jung, S., Hoernes, S., Mezger, K., 2000. Geochronology and petrogenesis of Pan-African, syn-tectonic, S-type and post-tectonic A-type granite (Namibia): products of melting of crustal sources, fractional crystallisation and wall rock entrainment. *Lithos* 50, 259-287.
- Kratinová, Z., Ježek, J., Schulmann, K., Hrouda, F., Shail, R.K., Lexa, O., 2010. Noncoaxial K-feldspar and AMS subfabrics in the Land's End granite, Cornwall: Evidence of magmatic fabric decoupling during late deformation and matrix crystallization. *Journal of Geophysical Research: Solid Earth* 115, 1-21.
- London, D., Manning, D.A.C., 1995. Chemical variation and significance of tourmaline from southwest England. *Economic Geology* 90, 495-519.
- Manning, D.A.C., Hill, P.I., 1990. The petrogenetic and metallogenetic significance of topaz granite from the southwest England orefield, in: Stein, H.J., Hannah, J.L. (Eds.), *Ore-bearing granite systems: petrogenesis and mineralizing processes*. Geological Society of American Special Paper, pp. 51-69.
- Manning, D.A.C., Hill, P.I., Howe, J.H., 1996. Primary lithological variation in the kaolinized St. Austell Granite, Cornwall, England. *Journal of the Geological Society* 153, 827-838.
- McDonough, W.F., Sun, S., 1995. The composition of the Earth. *Chemical Geology* 120, 223-253.
- Merino, E., Villaseca, C., Orejana, D., Jeffries, T., 2013. Gahnite, chrysoberyl and beryl co-occurrence as accessory minerals in a highly evolved peraluminous pluton: The Belvís de Monroy leucogranite (Cáceres, Spain). *Lithos* 179, 137-156.
- Monier, G., Robert, J.-L., 1986. Muscovite solid solutions in the system K₂O-MgO-FeO-Al₂O₃-SiO₂-H₂O: an experimental study at 2 kbar, P_{H₂O} and comparison with natural Li-free white micas. *Mineralogical Magazine* 50, 257-266.
- Montel, J.-M., Vielzeuf, D., 1997. Partial melting of metagreywackes, part II. Compositions of minerals and melts. *Contributions to Mineralogy and Petrology* 128, 176-196.
- Müller, A., Seltmann, R., Halls, C., Siebel, W., Dulski, P., Jeffries, T., Spratt, J., Kronz, A., 2006a. The magmatic evolution of the Land's End pluton, Cornwall, and associated pre-enrichment of metals. *Ore Geology Reviews* 28, 329-367.
- Müller, A., Thomas, R., Wiedenbeck, M., Seltmann, R., Breiter, K., 2006b. Water content of granitic melts from Cornwall and Erzgebirge: a Raman spectroscopy study of melt inclusions. *European Journal of Mineralogy* 18, 429-440.
- Nabelek, P.I., Bartlett, C.D., 1999. Fertility of metapelites and metagreywackes during leucogranite generation: an example from the Black Hills, USA, in: Barbarin, B., Stephens, W.E., Bonin, B., Bouchez, J.L., Clarke, D.B., Cuney, M., Martin, H. (Eds.), *Fourth Hutton Symposium: The origin of granites and related rocks*. Proceedings of a symposium held in Clermont-Ferrand, France, 20-25 September, 1999. GSA Books, USA.

- Nance, R.D., Gutiérrez-Alonso, G., Keppie, J.D., Linnemann, U., Murphy, J.B., Quesada, C., Strachan, R.A., Woodcock, N.H. 2010. Evolution of the Rheic Ocean. *Gondwana Research* 17, 194-222.
- Nance, R.D., Neace, E.R., Braid, J.A., Murphy, J.B., Dupuis, N., Shail, R.K., 2015. Does the Meguma Terrane Extend into SW England?, *Geoscience Canada* 42, 61-76.
- Neiva, A.M.R., Silva, P.B., Corfu, F., Ramos, J.M.F., 2011. Sequential melting and fractional crystallization: Granites from Guarda-Sabugal area, central Portugal. *Chemie der Erde - Geochemistry* 71, 227-245.
- Patiño-Douce, A.E., 1999. What do experiments tell us about the relative contributions of crust and mantle to the origin of granitic magmas? Geological Society, London, Special Publications 168, 55-75.
- Patiño-Douce, A.E., Harris, N.B.W., 1998. Experimental constraints on Himalayan anatexis. *Journal of Petrology* 39, 689-710.
- Patiño Douce, A.E., Johnston, A.D., 1991. Phase equilibria and melt productivity in the pelitic system: implications for the origin of peraluminous granitoids and aluminous granites. *Contributions to Mineralogy and Petrology* 107, 202-218.
- Pereira, M.D., Bea, F., 1994. Cordierite producing reactions at the Peña Negra Complex, Avila Batholith, central Spain: The key role of cordierite in low-pressure anatexis. *Canadian Mineralogist* 32, 763-780.
- Pichavant, M., Manning, D.A.C., 1984. Petrogenesis of tourmaline granites and topaz granites; the contribution of experimental data. *Physics of the Earth and Planetary Interiors* 35, 31-50.
- Pickering, J.M., Johnston, A.D., 1998. Fluid-absent melting behaviour of a two-mica metapelite: experimental constraints on the origin of Black Hills Granite. *Journal of Petrology* 39, 1787-1804.
- Pownall, J.M., Waters, D.J., Searle, M.P., Shail, R.K., Robb, L., 2012. Shallow laccolithic emplacement of the Land's End and Tregonning granites, Cornwall, UK: Evidence from aureole field relations and P-T modeling of cordierite-anthophyllite hornfels. *Geosphere* 8, 1467-1504.
- Raimbault, L., Cuney, M., Azencott, C., Duthou, J.L., Joron, J.L., 1995. Geochemical evidence for a multistage magmatic genesis of Ta-Sn-Li mineralisation in the granite at Beauvoir, French Massif Central. *Economic Geology* 90.
- Rieder, M., Cavazzini, G., D'Yakov, Y.S., Frank-Kamenetskii, V.A., Gottard, G., Guggenheim, S., Koval, P.V., Müller, G., Neiva, A.M.R., Radoslovich, E.W., Robert, J.-L., Sassi, F.P., Takeda, H., Weiss, Z., Wones, D.R., 1998. Nomenclature of the micas. *Canadian Mineralogist* 36, 41-48.
- Romer, R.L., Kroner, U., 2016. Phanerozoic tin and tungsten mineralization—Tectonic controls on the distribution of enriched protoliths and heat sources for crustal melting. *Gondwana Research* 31, 60-95
- Sawyer, E.W., Cesare, B., Brown, M., 2011. When the Continental Crust Melts. *Elements* 7, 229-234.
- Selwood, E.B., Durrance, E.M., Bristow, C.M., 1998. *The Geology of Cornwall*. University of Exeter Press, Exeter.
- Shail, R.K., Alexander, A.C., 1997. Late Carboniferous to Triassic reactivation of Variscan basement in the western English Channel: Evidence from onshore exposures in south Cornwall. *Journal of the Geological Society* 154, 163-168.
- Shail, R.K., Stuart, F.M., Wilkinson, J.J., Boyce, A.J., 2003. The role of post-Variscan extensional tectonics and mantle melting in the generation of the lower Permian granites and giant W-As-Sn-Cu-Zn-Pb orefield of SW England. *Transactions of the Institution of Mining and Metallurgy Section B: Applied Earth Science* 112, 127-129.
- Shail, R.K., Wilkinson, J.J., 1994. Late-to post-Variscan extensional tectonics in south Cornwall. *Proceedings of the Ussher Society* 8, 262-270.
- Sheppard, S.M.F. 1977. The Cornubian Batholith, SW England: D/H and $^{18}\text{O}/^{16}\text{O}$ studies of kaolinite and other alteration minerals, *Journal of the Geological Society of London* 133, 575-591.
- Spear, F.F., Kohn, M.J., Cheney, J.T., 1999. P-T paths from anatexis pelites. *Contributions to Mineralogy and Petrology* 134, 17-32.
- Štemprok, M., Seifert, T., 2010. The association of lamprophyric intrusions and rare-metal mineralisation. *Mineralogia Special Papers* 37, 61-62.

- Stimac, J.A., Clark, A.H., Chen, Y., Garcia, S., 1995. Enclaves and their bearing on the origin of the Cornubian Batholith, southwest England. *Mineralogical Magazine* 59, 273-296.
- Stone, M., 1975. Structure and petrology of the Tregonning-Godolphin Granite, Cornwall. *Proceedings of the Geologist's Association* 86, 155-170.
- Stone, M., 1992. The Tregonning Granite: petrogenesis of Li-mica granites in the Cornubian Batholith. *Mineralogical Magazine* 56, 141-155.
- Stone, M., 2000. The early Cornubian plutons: a geochemical study, comparisons and some implications. *Geoscience in southwest England* 10, 37-41.
- Stone, M., Exley, C.S., George, M.C., 1988. Compositions of trioctahedral micas in the Cornubian Batholith. *Mineralogical Magazine* 52, 175-192.
- Sylvester, P.J., 1998. Post-collisional strongly peraluminous granites. *Lithos* 45, 29-44.
- Tartèse, R., Boulvais, P., 2010. Differentiation of peraluminous leucogranites "en route" to the surface. *Lithos* 114, 353-368.
- Taylor, G.K., 2007. Pluton shapes in the Cornubian Batholith: New perspectives from gravity modelling. *Journal of the Geological Society* 164, 525-528.
- Taylor, R.P., 1992. Petrological and geochemical characteristics of the Pleasant Ridge zinnwaldite - topaz granite, southern New Brunswick, and comparisons with other topaz-bearing felsic rocks. *Canadian Mineralogist* 30, 895-921.
- Teixeira, R.J.S., Neiva, A.M.R., Gomes, M.E.P., Corfu, F., Cuesta, A., Croudace, I.W., 2012. The role of fractional crystallization in the genesis of early syn-D3, tin-mineralized Variscan two-mica granites from the Carrazeda de Ansiães area, northern Portugal. *Lithos* 153, 177-191.
- Thorpe, R.S., 1987. Permian K-rich volcanic rocks of Devon: petrogenesis, tectonic setting and geological significance. *Transaction of the Royal Society of Edinburgh: Earth Sciences* 77, 361-366.
- Tischendorf, G., Gottsmann, B., Forster, H.-J., Trumbull, R.B., 1997. On Li-bearing micas: estimating Li from electron microprobe analyses and an improved diagram for graphical representation. *Mineralogical Magazine* 61, 809-834.
- Vielzeuf, D., Montel, J.M., 1994. Partial melting of metagreywackes. Part I. Fluid-absent experiments and phase relationships. *Contributions to Mineralogy and Petrology* 117, 375-393.
- Villaseca, C., Pérez-Soba, C., Merino, E., Orekana, D., López-García, J.A., Billstrom, K., 2008. Contrasting crustal sources for peraluminous granites of the segmented Montes de Toledo Batholith (Iberian Variscan Belt). *Journal of Geosciences* 53, 263-280.
- Ward, C.D., McArthur, J.M., Walsh, J.N., 1992. Rare earth element behaviour during evolution and alteration of the Dartmoor Granite, SW England. *Journal of Petrology* 33, 785-815.
- Warr, L.N., Primmer, T.J., Robinson, D., 1991. Variscan very low-grade metamorphism in southwest England: a diastathermal and thrust-related origin. *Journal of Metamorphic Geology* 9, 751-764.
- Watson, E.B., Harrison, T.M., 1983. Zircon saturation revisited: temperature and composition effects in a variety of crustal magma types. *Earth and Planetary Science Letters* 64, 295-304.
- Williamson, B.J., Müller, A., Shail, R.K., 2010. Source and partitioning of B and Sn in the Cornubian Batholith of southwest England. *Ore Geology Reviews* 38, 1-8.
- Willis-Richards, J., Jackson, N.J., 1989. Evolution of the Cornubian ore field, southwest England: Part I. Batholith modeling and ore distribution. *Economic Geology* 84, 1078-1100.
- Wolf, M.B., London, D., 1994. Apatite dissolution into peraluminous haplogranitic melts: An experimental study of solubilities and mechanisms. *Geochimica et Cosmochimica Acta* 58, 4127-4145.
- Yu, Z., Robinson, P., McGoldrick, P., 2001. An evaluation of methods for the chemical decomposition of geological materials for trace element determination using ICP-MS. *Geostandards Newsletter* 25, 199-217.
- Ziegler, P.A., Dèzes, P., 2006. Crustal evolution of Western and Central Europe. *Geological Society, London, Memoirs* 32, 43-56.

Table 1

Granite	Two-mica (G1)	Muscovite (G2)	Biotite (G3)	Tourmaline (G4)	Topaz (G5)
Macroscopic features	Fine- to coarse- grained , variably common (<5-25%) Kfs phenocrysts (<25 mm), Bt ≈Msc, whitish grey	Fine- to coarse-grained, variably common (<5-25%) Kfs phenocrysts (<25 mm), Msc > Bt, whitish grey	Medium- to coarse- grained, common (15-25%) Kfs phenocrysts (>25 mm), Bt > Msc, grey	Fine- to medium- grained, variable Kfs and Qtz phenocrysts (>25 mm), Bt > Msc, grey to pinkish grey	Medium-grained, equigranular, rare Kfs phenocrysts, Tz as major mineral, white
Major mineralogy	Qtz, microperthitic Kfs, Pl (An ₁₅₋₃₀), Mg siderophyllite, Msc. Bt ≈ Msc, Kfs > Pl	Qtz, microperthitic Kfs, Pl(An ₁₀), Msc, Li siderophyllite. Msc > Bt, Kfs > Pl	Qtz, microperthitic Kfs, Pl (An ₁₅₋₃₀), magnesium siderophyllite, Tur, Crd. Kfs ≈ Pl, Bt > Tur	Qtz, microperthitic Kfs, pl (An ₄₈), Tur, Zwd. Tur ≠ or > Bt, Kfs ≈ Pl	Qtz, microperthitic Kfs, Pl (An ₄₅), Lpd, Tz, Tur. Pl > Kfs
Accessory minerals	Tur, And, Ap, Zrc, Mon, Rt, Ilm, Xt, Mon, Py	Tur, Tz, Ap, Zrc, Rt, Ilm, Fl.	Msc, Zrc, Ap, Rt, Ilm, Mon, Xt, Py.	Msc, Tz, Ap, Zrc, Fl, (Nb,Ta-)Rt, Ilm, Th, phosphates.	Ap, (Nb-)Rt, Ilm, Msc, Zrc, phosphates.
Age (Ma ± 2σ)	291.4 ± 1.6 ¹ – 281.5 ± 1.6 ²	298.3 ± 4.6 ² – 279.3 ± 0.8 ¹	281.8 ± 0.8 ¹ – 272.3 ± 1.8 ¹	Unknown	281 ± 1.3 ²
Occurrence	Major composite plutons (Bodmin, Carmmenellis, Isles of Scilly)	Small stocks associated with NW-SE trending faults	Major composite plutons (Land's End, Dartmoor)	Small stocks, spatially associated with G3	Small stocks associated with NW-SE trending faults
Enclaves	Metasedimentary	None seen	Metasedimentary, mafic microgranular	Mafic microgranular	Metasedimentary
Other features	Strained quartz widespread	Some stocks associated with greisen deposits	Qtz-Tur orbicules common	Variable textures see Manning <i>et al.</i> (1996)	Associated with aplites (e.g. Megiliggar Rocks)

Abbreviations: And – andalusite; Ap – apatite; Bt – biotite; Crd – cordierite; Fl – fluorite; Ilm – ilmenite; Kfs – alkali feldspar; Lpd – Lepidolite; Mon – monazite; Msc – muscovite; Pl – plagioclase; Py – Pyrite; Qtz – quartz; Rt – rutile; Th – thorite; Tur – tourmaline; Tz – topaz; Xt – xenotime; Zrc – zircon; Zwd – Zinnwaldite. ¹U-Pb monazite Chesley *et al.* (1993); ²Ar-Ar muscovite Clark *et al.* (1994).

Table 2

	G1	G2	G3	G4	G5
Plagioclase core					
Or	2.1	1.5	3.4	1.3	0.8
Ab	82.6	94.3	84.0	95.9	98.6
An	15.3	4.1	12.7	2.8	0.6
Plagioclase rim					
Or	2.0	1.1	1.3	0.6	0.7
Ab	83.7	97.2	97.6	98.5	98.5
An	14.3	1.8	1.1	0.9	0.8
Orthoclase					
Or	92.0	93.8	95.0	93.9	92.8
Ab	7.9	6.1	4.9	6.1	7.2
An	0.1	0.1	0.1	0.0	0.0

Table3

	Detecti on limit	G1a	G1b	G1c	G2	G3a	G3c	G3d	G4a	G4b	G4c	G5a	G5b
Major elements (wt. %)													
SiO ₂	0.01	71.83	71.95	72.34	72.26	71.61	73.59	72.17	73.22	73.37	72.59	71.81	72.43
Al ₂ O ₃	0.01	14.71	14.84	14.77	14.79	14.26	13.40	0.09	15.03	14.24	14.40	16.08	0.04
TiO ₂	0.01	0.24	0.21	0.20	0.15	0.31	0.23	14.94	0.09	0.12	0.15	0.06	15.90
Fe ₂ O ₃	0.01	1.70	1.61	1.58	1.27	2.33	1.82	0.88	1.04	1.29	1.66	1.15	0.59
MnO	0.001	0.03	0.04	0.02	0.03	0.04	0.04	0.01	0.01	0.02	0.03	0.04	0.11
MgO	0.01	0.41	0.40	0.33	0.25	0.50	0.35	0.27	0.12	0.15	0.20	0.10	0.02
CaO	0.01	0.70	0.75	0.60	0.48	0.73	0.47	1.69	0.67	0.53	0.44	0.47	0.47
Na ₂ O	0.01	2.70	2.93	2.81	2.62	2.82	3.11	2.66	3.41	3.21	2.94	3.68	4.15
K ₂ O	0.01	5.51	5.28	5.29	6.00	5.25	5.05	4.70	4.64	4.75	4.94	4.47	3.74
P ₂ O ₅	0.01	0.23	0.22	0.19	0.24	0.23	0.19	0.40	0.39	0.33	0.29	0.46	0.40
LOI		1.31	1.23	1.44	1.29	1.21	0.90	1.83	1.35	1.17	1.36	1.44	1.43
Sum		99.36	99.46	99.56	99.36	99.23	99.15	99.62	99.93	99.17	98.99	99.75	99.24
Trace elements (ppm)													
Ba	5	213	233	385	178	218	161	35	68	63	78	32	18
Pb	5	38	34	35	19	26	28	<5	<5	10	13	9	9
Rb	2	424	430	379	584	429	362	175	657	732	712	1138	1630
Sr	2	95	96	100	55	82	52	27	51	32	38	38	35
Nb		10	11	14	15	17	12	12	29	30	26	54	54
Th	6	18	16	40	10	21	15	3	<6	9	11	<6	<6
U	5	8	8	<5	6	10	8	10	<5	6	20	19	7
Zr	5	104	97	129	66	147	103	42	39	52	73	25	18
REE (ppm)													
La	0.3	21.45	19.50	21.97	11.25	20.64	10.96	3.21	3.24	5.96	9.26	1.22	0.43
Ce	0.6	43.88	40.07	43.13	23.38	43.77	21.52	6.70	6.62	12.75	21.12	2.50	0.36
Pr	0.3	5.41	4.80	5.42	2.99	5.79	2.85	1.05	0.81	1.64	2.64	0.36	0.37
Nd	0.3	19.17	17.13	19.05	10.75	21.49	10.47	4.42	2.90	5.89	9.80	1.30	0.37
Sm	0.3	3.77	3.42	3.43	2.26	4.39	2.24	1.46	0.64	1.32	2.07	0.45	0.31
Eu	0.03	0.41	0.32	0.31	0.25	0.37	0.11	0.13	0.06	0.06	0.11	0.03	0.08
Gd	0.1	2.48	2.32	2.18	1.70	3.18	1.62	1.52	0.56	1.03	1.43	0.49	0.20
Dy	0.2	1.41	1.27	1.38	1.35	2.23	1.31	1.60	0.62	0.92	0.96	0.58	0.22
Ho	0.08	0.23	0.20	0.23	0.24	0.38	0.23	0.28	0.12	0.16	0.16	0.12	0.21
Er	0.05	0.52	0.50	0.59	0.63	0.99	0.66	0.79	0.35	0.44	0.44	0.28	0.21
Tm	0.04	0.08	0.07	0.09	0.09	0.14	0.10	0.12	0.06	0.07	0.07	0.05	0.19
Yb	0.1	0.52	0.43	0.53	0.60	0.89	0.69	0.86	0.43	0.49	0.47	0.33	0.22
Lu	0.03	0.08	0.06	0.08	0.09	0.14	0.11	0.12	0.07	0.08	0.07	0.06	0.24
A/CNK		1.26	1.25	1.30	1.27	1.23	1.17	1.19	1.27	1.25	1.32	1.38	1.36
Eu/Eu*		0.41	0.35	0.36	0.37	0.29	0.18	0.27	0.28	0.15	0.21	0.11	0.82
Rb/Sr		4.66	4.65	4.98	11.66	6.96	6.96	6.51	13.84	31.01	19.13	36.84	61.05
K/Rb		108	104	123	84	104	116	223	59	58	58	35	20
TZr (°C)		775	768	775	737	802	773	691	751	720	748	675	648

*Note all Fe as Fe₂O₃

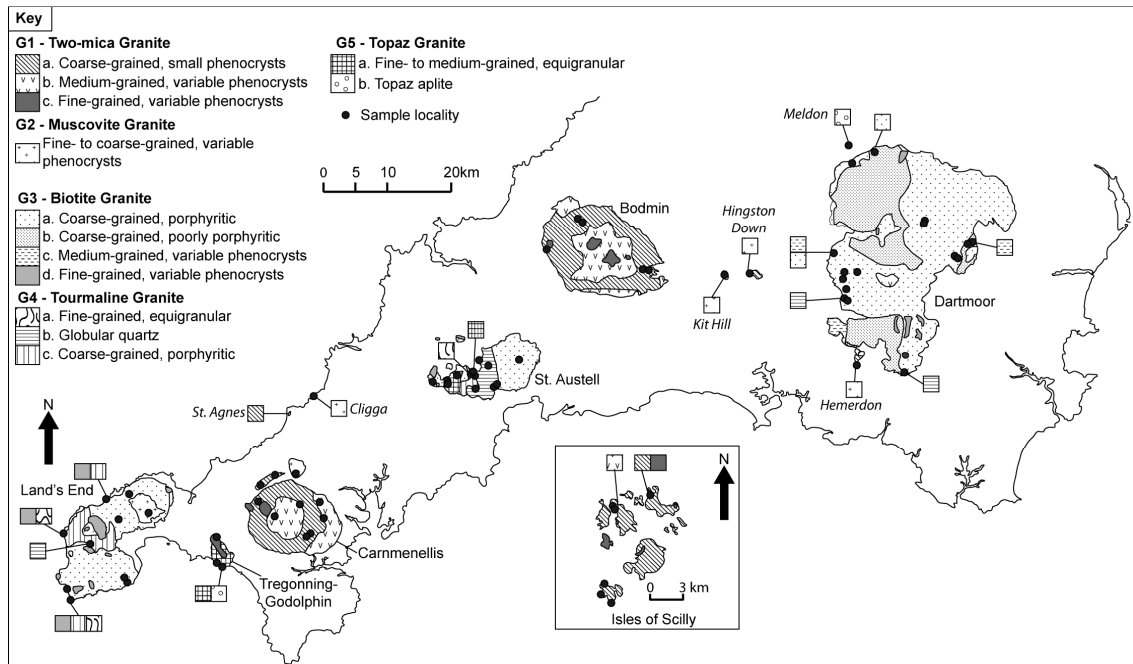


Figure 1



Figure 2

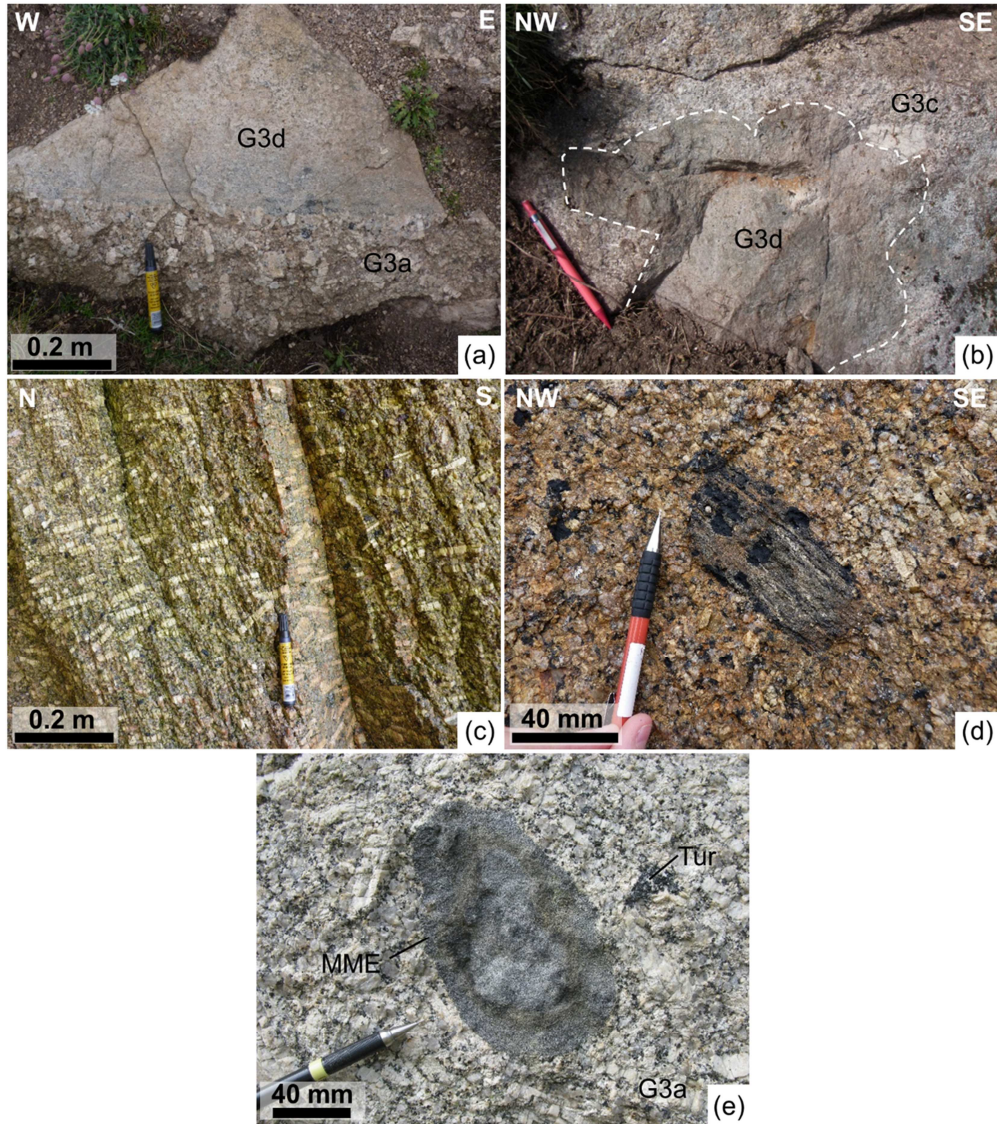


Figure 3

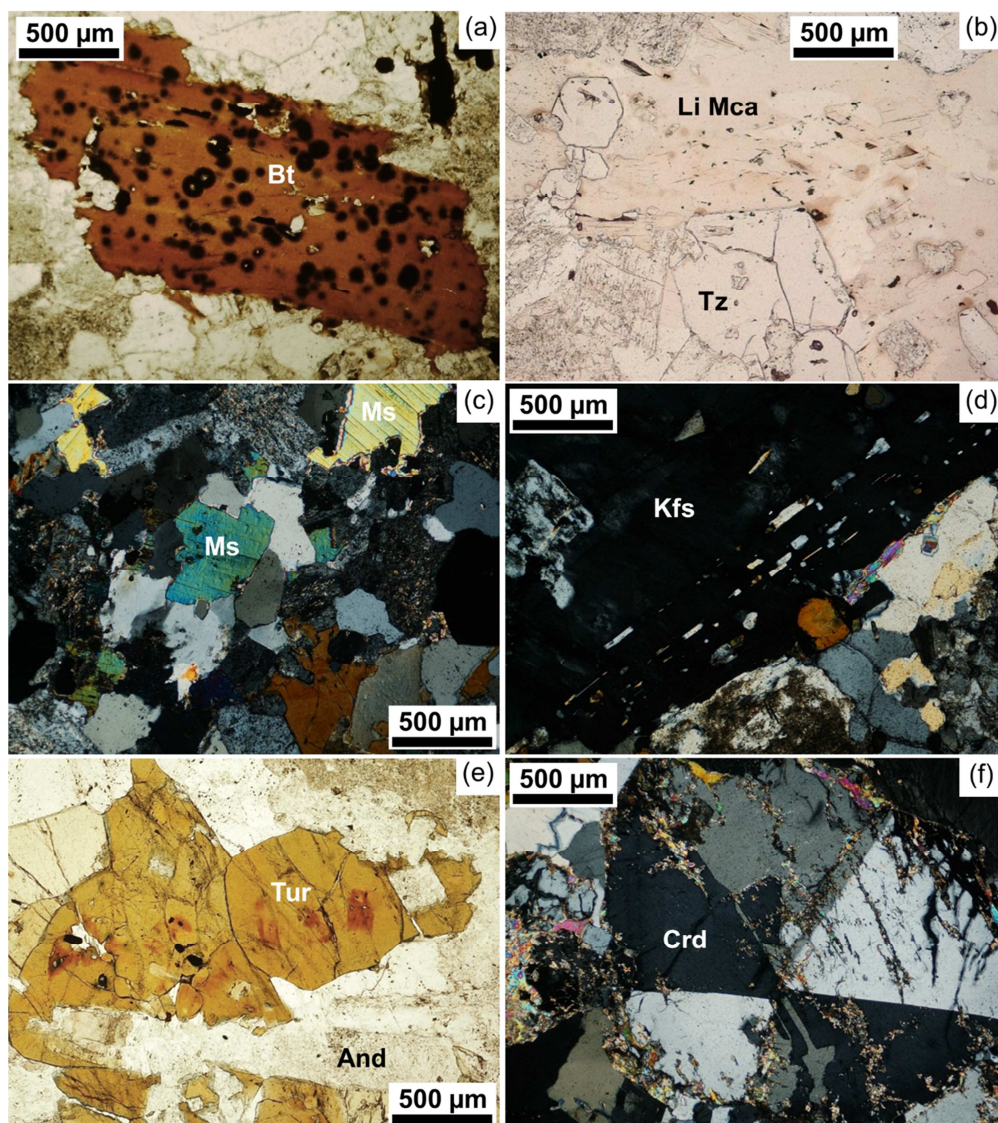


Figure 4

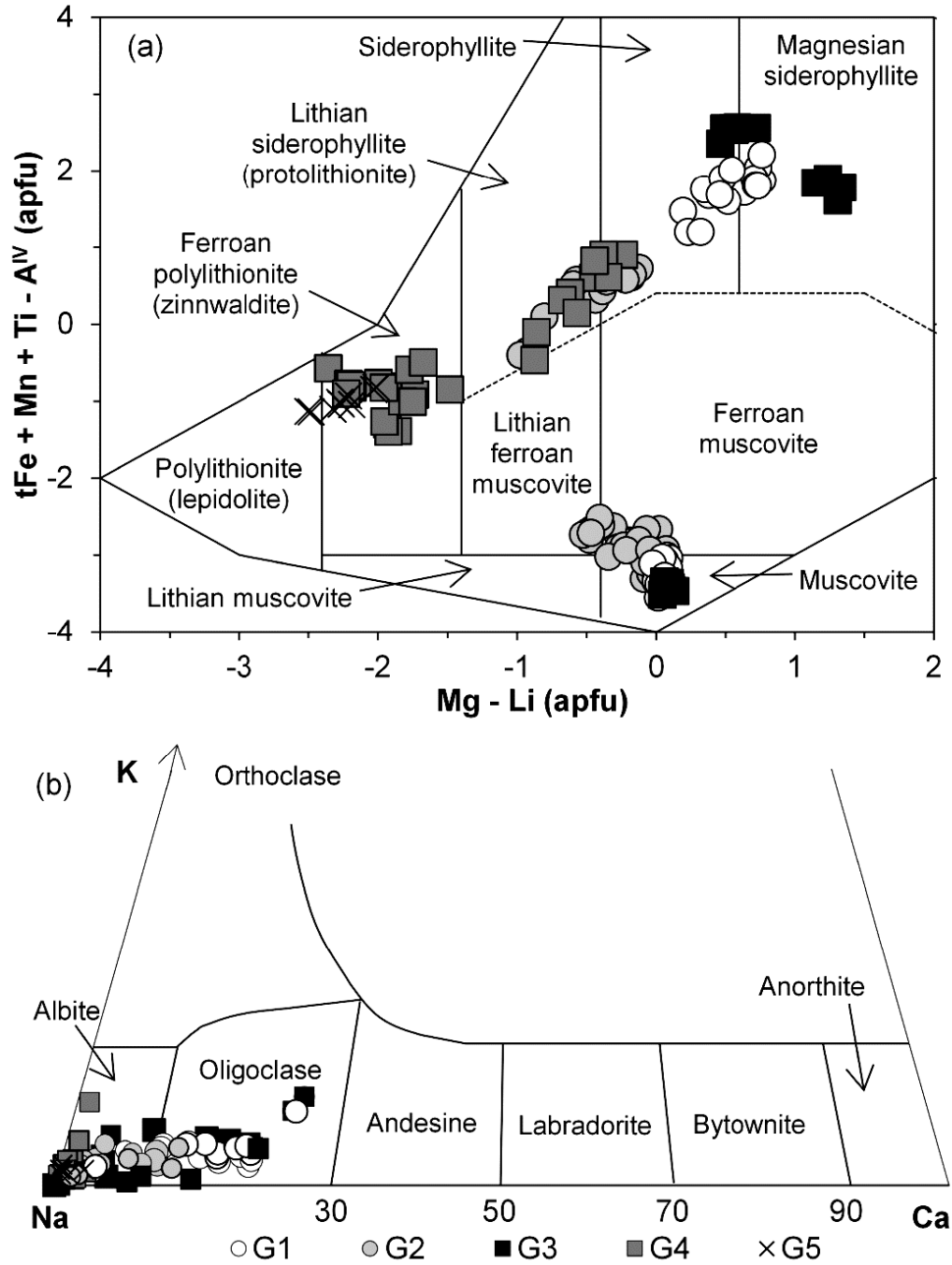


Figure 5

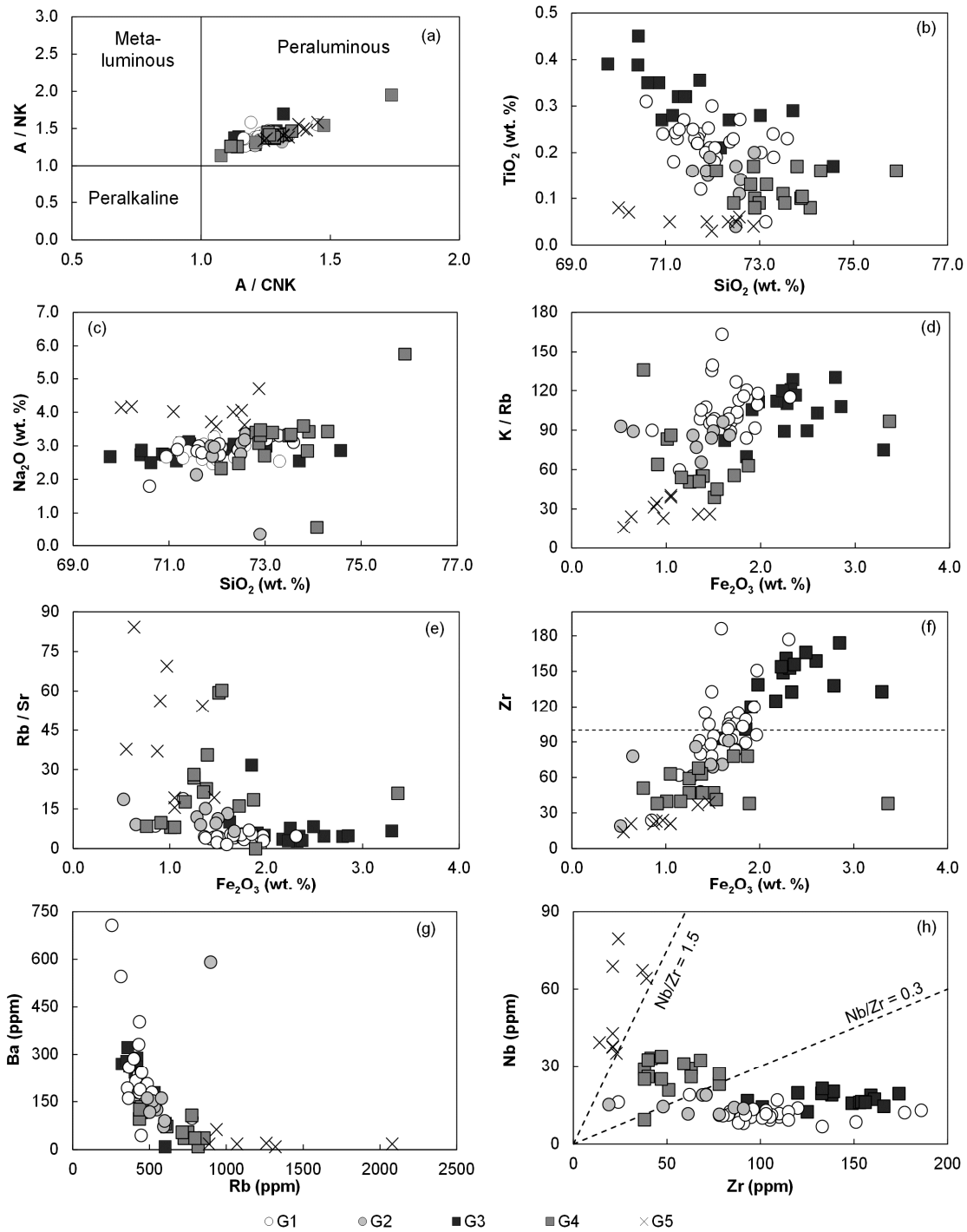


Figure 6

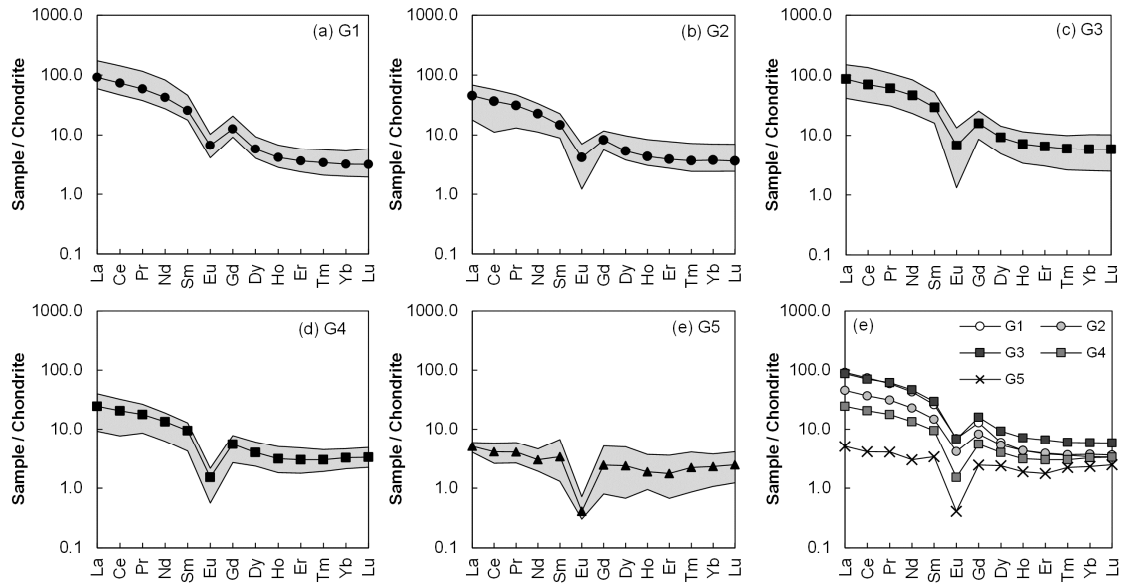


Figure 7

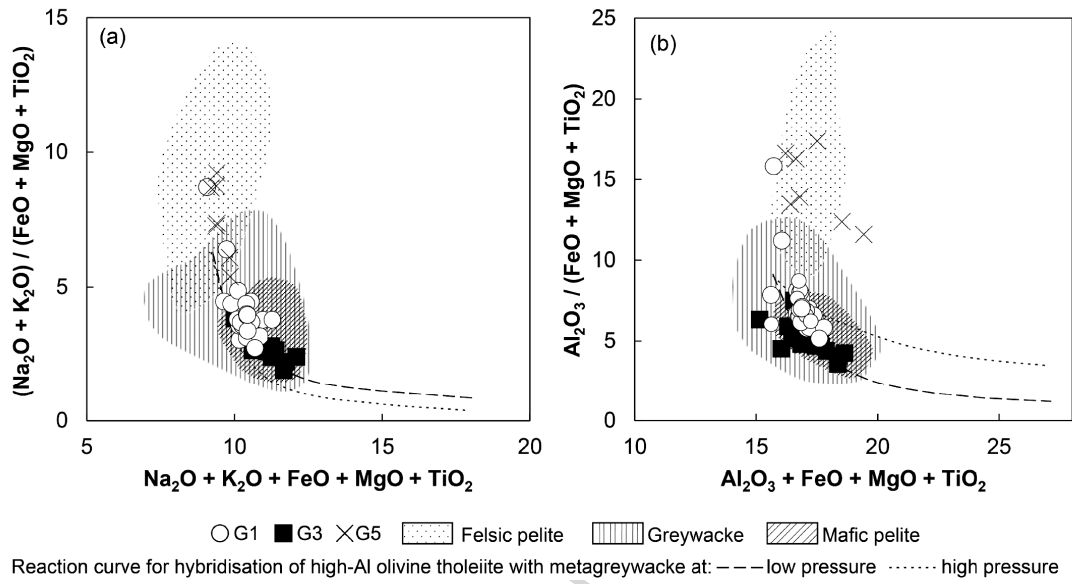


Figure 8

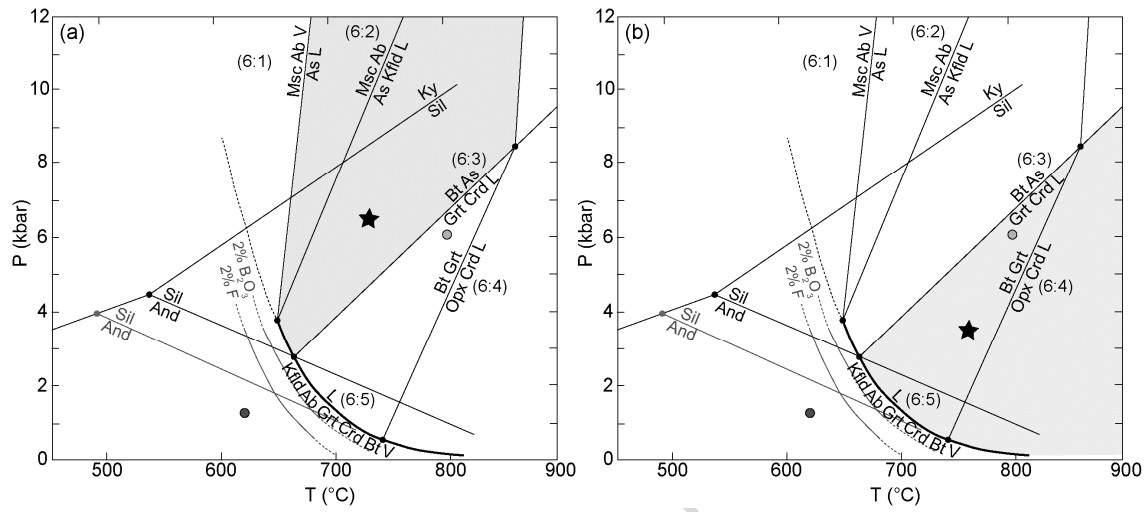


Figure 9

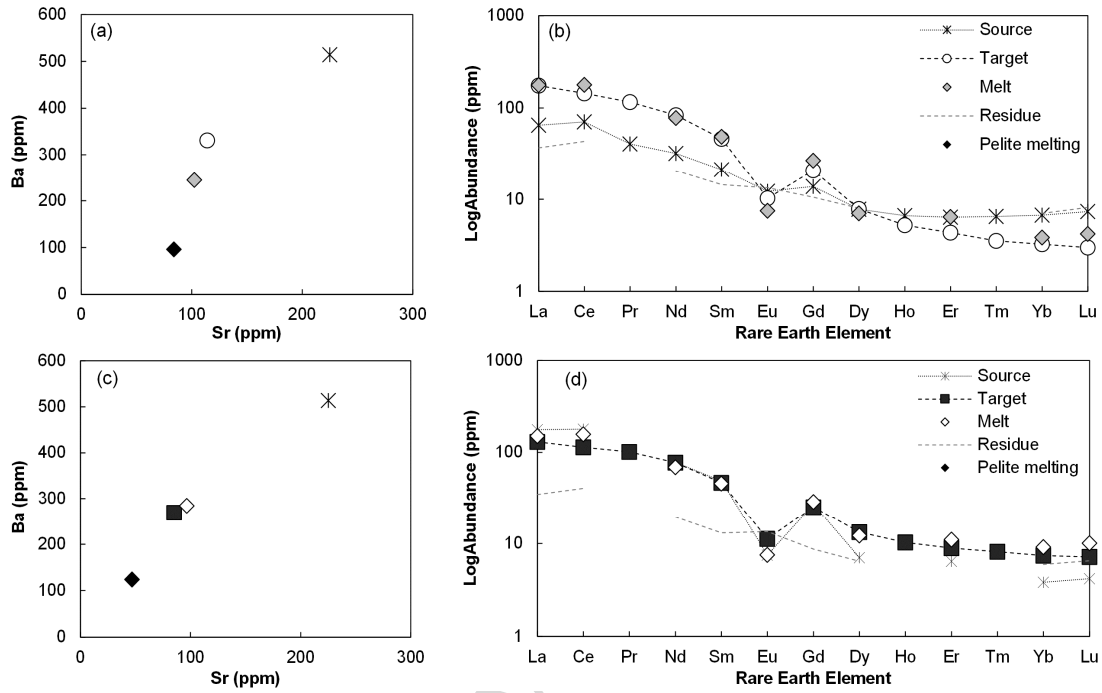


Figure 10

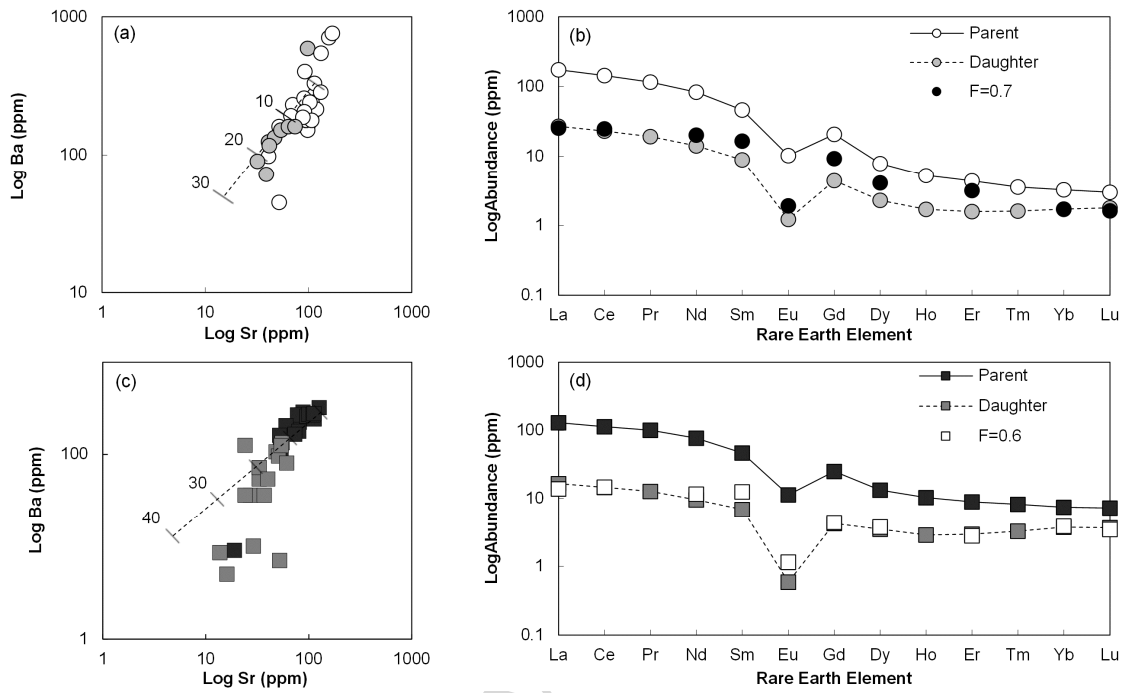


Figure 11

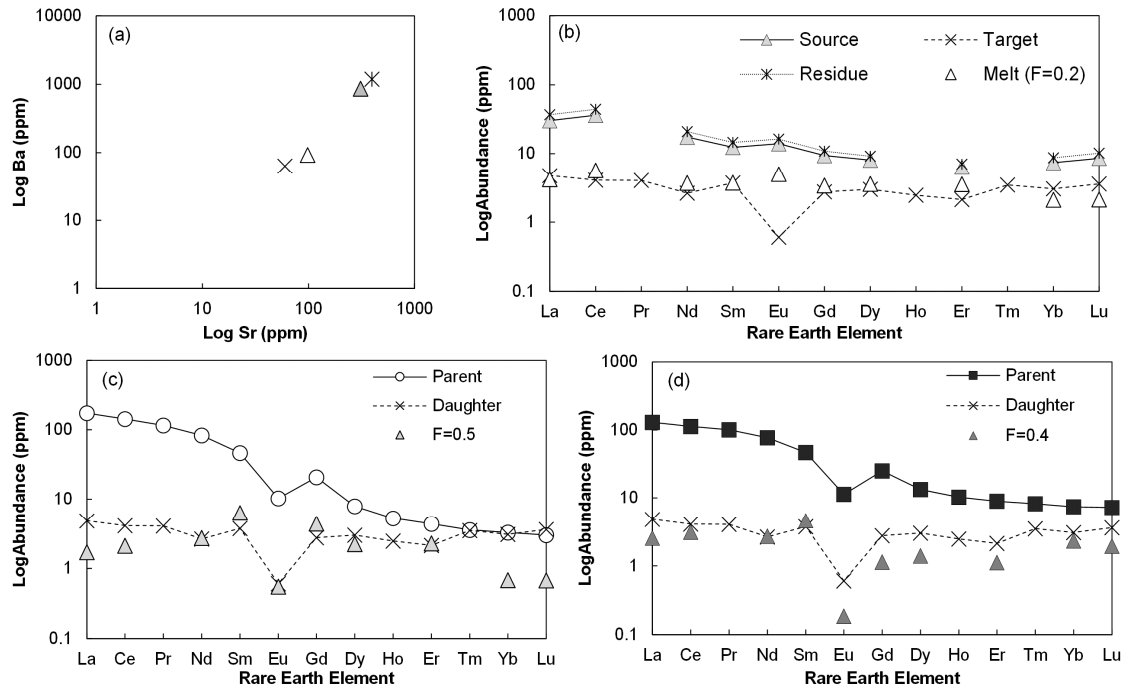


Figure 12

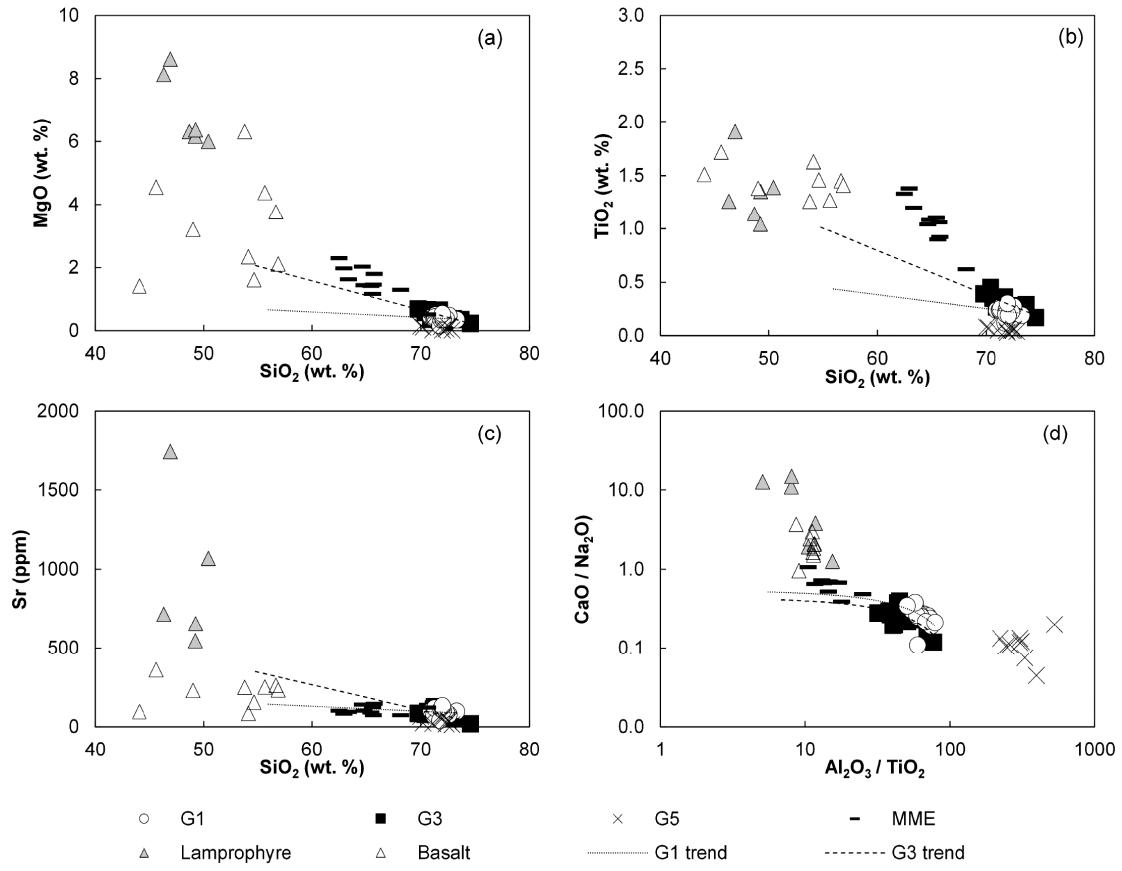


Figure 13

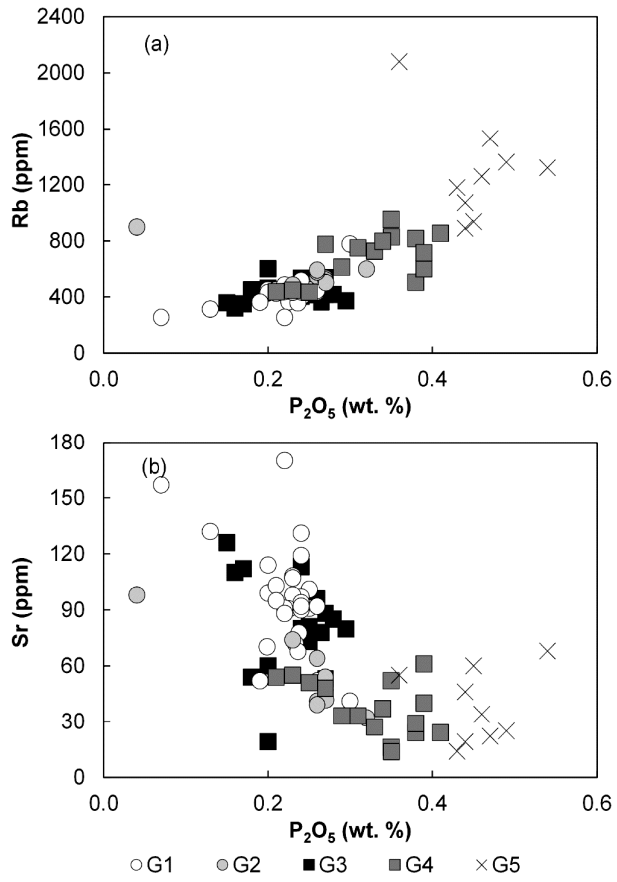
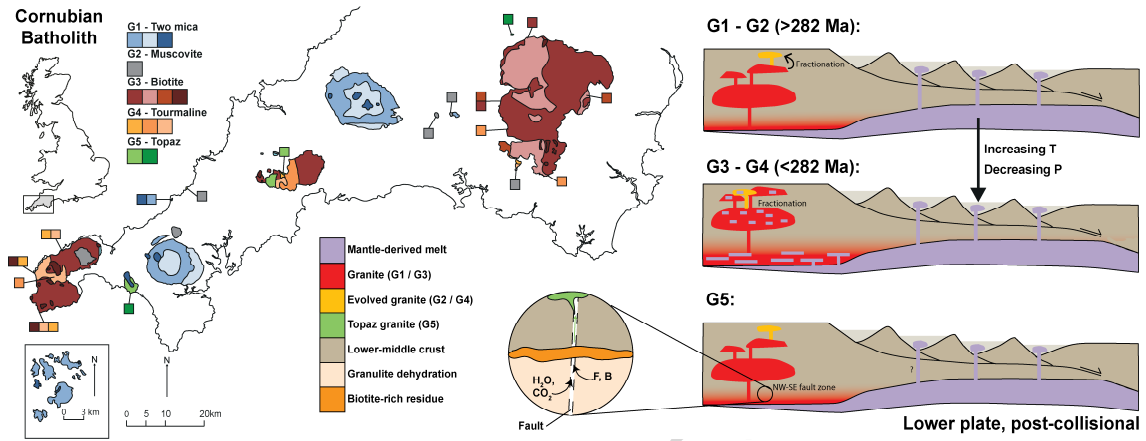


Figure 14



Graphical abstract

Highlights

- Petrogenesis of post-Variscan peraluminous granites in the Cornubian Batholith.
- Geochemistry, mineralogy, mineral chemistry and modelling define 5 granite groups.
- G1 and G3 formed by partial melting of a metagreywacke with a minor mantle component.
- G5 is derived from fluid-fluxed melting of biotite-rich restite in the lower crust.